The role of mixing in the large-scale ocean circulation

Casimir de Lavergne, Sjoerd Groeskamp, Jan Zika, Helen L Johnson

The role of mixing in the large-scale ocean circulation

C. de Lavergne,[1] S. Groeskamp,[2] J. Zika,[3] H. L. Johnson[4]

[1]LOCEAN Laboratory, Sorbonne Université-CNRS-IRD-MNHN,
Paris F-75005, France
[2]NIOZ Royal Netherlands Institute for Sea Research, P.O. Box 59, 1790 AB,
Den Burg, Texel, The Netherlands
[3]School of Mathematics and Statistics, University of New South Wales,
Sydney, Australia
[4]Department of Earth Sciences, University of Oxford,
Oxford, United Kingdom

Abstract

Irreversible mixing of tracers and momentum in the ocean occurs via diffusion and friction at the scale of molecules. That such molecular processes profoundly influence basin-scale ocean currents is counter-intuitive. Many successful theories of ocean circulation indeed ignore diffusive and frictional processes. Yet oceanographers have long recognized that turbulence can amplify irreversible mixing and its influence on large-scale flows. In recent years, substantial progress has been made in the mapping of mixing energized by three-dimensional and geostrophic turbulence. This progress not only helps to quantify connections between mixing and observed circulation systems, but also to better characterize these circulation systems. This chapter surveys the rapidly evolving understanding of the impacts of mixing on the strength and structure of major ocean gyres, overturning circulations and the Antarctic Circumpolar Current. Accumulating evidence suggests that global ocean circulation is shaped by energetic mixing near ocean boundaries, while either weak or largely adiabatic away from boundaries.

Keywords

Ocean circulation, currents, gyre, overturning, mixing, turbulence

1. Introduction

At low latitudes, the Earth receives more heat from the Sun than it radiates out to space over an annual orbit. The opposite occurs at high latitudes, where outgoing longwave radiation exceeds incoming shortwave insolation. This latitudinal contrast is the primary driving force of coupled atmosphere and ocean circulations. It is imprinted on the ocean surface, which gains heat at low latitudes and loses heat to the atmosphere at higher latitudes. This differential surface heating of the ocean generates and amplifies the contrast between warm tropical waters and colder waters that fill higher latitude and deep basins (Fig. 1). To counteract the tendency to warm warm waters and cool cold waters, the ocean must transfer heat from low to high latitudes.

Such transfer can be achieved by moving warm surface water into the region of surface heat loss, thus evacuating heat from the warm bowl and reducing exposure to cooling of the cold pool (Fig. 1a,b). This advective scenario implies a permanent or transient deformation or displacement of the warm bowl so that it stretches into the cooling latitudes. Compensating equatorward flow of colder waters can occur in the horizontal plane, establishing a horizontal circulation, such as a gyre or an eddy (Fig. 1a). Alternatively the compensating flow may take place in the vertical plane, leading to an overturning circulation, such as an inter-hemispheric overturning (Fig. 1b). By shifting water bodies along the meridional axis, horizontal and overturning circulations can thus mitigate the imbalance implied by the latitudinal contrast in surface heat fluxes.

The scenarios described above invoke exclusively advection (i.e., mass transport) and surface heat fluxes, implicitly assuming that the ocean interior is devoid of non-advective heat fluxes or is *adiabatic*. The opacity of seawater does prevent solar heating from penetrating significantly

deeper than 200 m. However, heat exchanges are not restricted to the sunlit surface layer. Through temperature diffusion or *mixing*, heat can be transferred between water bodies in the ocean interior. If diffusion is able to transfer heat from the warm bowl to the cold pool at a rate similar to the net low-latitude surface heat gain, the idealised two-layer ocean of Fig. 1 may achieve heat balance via mixing rather than circulation (Fig. 1c).

A recent calculation of mixing-induced heat transfer across temperature classes in a realistic ocean model finds that the peak transfer, estimated at 1.6 PW across the 22°C isotherm, is of similar magnitude to the peak poleward oceanic heat transport (Holmes et al. 2018a, 2019). This result suggests that mixing plays a central role in maintaining heat balance against differential surface heating. Does it imply that the diffusive scenario of Fig. 1c dominates over advective scenarios of Fig. 1a,b? The reality is more subtle, because advection and diffusion are not independent processes, and indeed combine to shape oceanic transports of mass and heat. For example, the presence of a diffusive heat supply to the cold pool may allow hemispheric overturning circulations to develop (Fig. 1d). These circulations depend upon the existence of mixing, and contribute to poleward heat transport.

Coupling between advection and diffusion is ubiquitous. Any mass transport that crosses isosurfaces of a conservative tracer (e.g., surfaces of constant salinity) below the ocean surface requires mixing. Mixing of momentum also exerts a profound, direct influence on ocean currents. Conversely, mixing rates often depend on surrounding currents, and more specifically on the turbulent motions that stir the ocean. Indeed, over most of the ocean, turbulence elevates effective mixing rates well above the weak molecular diffusivities. Mass transports thus contribute to amplify mixing via turbulence. This implies that mixing and advection rely on shared sources of kinetic energy, ultimately derived from surface winds, surface buoyancy fluxes, tides,

and geothermal heating (Fig. 2). Understanding the role of mixing in global ocean circulation requires (i) quantifying mixing rates by tracking energy from external sources to turbulence to mixing, and (ii) identifying the upscale influence of turbulent mixing on large-scale current systems.

In this chapter, we will focus on current systems spanning thousands of kilometers: basin-scale ocean gyres, the Antarctic Circumpolar Current and subtropical and deep overturning circulations. We begin with an overview of mixing processes and their mathematical representation (section 2). We next examine features of the large-scale ocean circulation that can be understood without consideration of mixing (section 3). The discussion of the impacts of mixing focuses by turns on mechanisms (section 4), their distribution (section 5), and their consequences for observed overturning (section 6) and horizontal (section 7) circulations. The emerging view is that of a relatively adiabatic interior ocean circulation commanded by strongly mixing boundaries (section 8).

2. Flavours of mixing

Ocean flows are governed by the Navier-Stokes equations on a rotating sphere. The equations determine the evolution of the three-dimensional velocity vector $\vec{u} = (u, v, w)$ as a function of inertial, pressure gradient, gravitational, Coriolis and frictional forces:

$$\frac{\partial \vec{u}}{\partial t} + \vec{u} \cdot \nabla \vec{u} = -\frac{1}{\rho} \nabla p + \vec{g} - f \vec{z} \times \vec{u} + \nabla \cdot \nu \nabla \vec{u} \tag{1}$$

where we have made the traditional approximation; that is, we neglected the vertical component of the Coriolis force. In (1), p is pressure, ρ density, $\vec{g}$ the gravity vector, f the Coriolis parameter, $\vec{z}$ the vertical unit vector, ν the molecular kinematic viscosity of seawater, and ∇ the three-

dimensional gradient operator. The last term represents the divergence of the down-gradient momentum transfer achieved by frictional interactions between water molecules. Assuming no sources and sinks of momentum at ocean boundaries, it can be shown that this term leaves the average momentum over the whole ocean volume unchanged but decreases the global variance of momentum. These two integral properties are fundamental characteristics of diffusion.

Equation (1) does not suffice to characterise the evolution of the fluid. It must be complemented by the continuity equation (expressing mass conservation), an equation of state relating density to pressure, temperature and salinity, and evolution equations for conservative temperature Θ and absolute salinity S_A (McDougall 2003, McDougall et al. 2012). The latter two equations are analogous to that governing the evolution of an arbitrary tracer C,

$$\frac{\partial C}{\partial t} + \vec{u} \cdot \nabla C = Q_C + \nabla \cdot \kappa_C \nabla C, \tag{2}$$

where Q_C encapsulates interior sources and sinks and κ_C is the molecular diffusivity of C. A conservative tracer has $Q_C \equiv 0$; this is the case for conservative temperature (except for sub-surface solar heating) and absolute salinity. Boundary fluxes of C enter as boundary conditions on the last term in (2). In the absence of such fluxes, this diffusion term preserves the domain average C and decreases the domain-wide variance of C. The reduction of variance can be illustrated with the idealised heat balance of Fig. 1c: diffusion acts to reduce the temperature contrast between the two layers, hence to diminish global temperature variance, whereas surface forcing acts in the opposite sense. More generally, boundary fluxes are the only means to increase global variance of a conservative tracer, implying that mixing and boundary fluxes are intrinsically tied in this variance competition (Walin 1977, 1982, Zika et al. 2015).

Can the diffusive terms $\nabla \cdot \nu \nabla \vec{u}$, $\nabla \cdot \kappa_\Theta \nabla \Theta$ and $\nabla \cdot \kappa_{S_\mathrm{A}} \nabla S_\mathrm{A}$ affect the large-scale distribution

of momentum $\vec{u}$? Molecular diffusion coefficients ν, κ_Θ and κ_{S_A} vary little about respective values of 1×10^{-6}, 1.4×10^{-7} and 1.4×10^{-9} m^2 s^{-1}. The characteristic time to diffuse a momentum anomaly from the surface to 4 km depth follows as $(4000\text{m})^2/\nu = 16 \times 10^{12}$ s or about 500,000 years. Equivalent timescales for heat and salt are respectively one and three order(s) of magnitude larger. It is immediately apparent that molecular diffusivities are far too weak to affect global circulation systems known to evolve on timescales of seasons to millennia. Scaling frictional and Coriolis terms in (1) further shows that, for a typical value of $f \sim 10^{-4}$ s^{-1}, the two terms are comparable at length scales of 10^{-1} m. Only at length scales smaller than 10 centimetres do molecular processes become considerable.

Using fast probes able to measure velocity and temperature variations at centimetre scale, it is possible to estimate the rate of molecular dissipation of kinetic energy ($-\nu(\nabla\vec{u})^2$) and temperature variance ($-\kappa_\Theta(\nabla\Theta)^2$) along a vertical cast in the ocean (Osborn and Cox 1972, Osborn 1978, Chapter 14). Such measurements show that the ocean is strewn with small patches of elevated shear and temperature microstructure (Gregg 1987). The magnitude and distribution of the measured micro-scale gradients cannot be explained by large-scale momentum and temperature variations: they arise from intermittent turbulent motions. These motions stir large-scale gradients and produce small-scale variance that is ultimately dissipated by molecular interactions. As a result, molecular dissipation of momentum and temperature variance is typically several orders of magnitude larger than would be expected in a laminar ocean (Gargett and Osborn 1981, Oakey 1982).

Stirring by motions of intermediate scale—-between major currents spanning thousands of kilometres and molecular processes acting over centimetres—thus accelerates the downscale cascade of variance and amplifies the gradients upon which molecular viscosity and diffusivities

act. The ability of turbulence to amplify mixing becomes apparent in equations (1) and (2) when a Reynolds decomposition of variables into mean and fluctuating components is performed: $\vec{u} = \overline{\vec{u}} + \vec{u'}$, $C = \overline{C} + C'$, and so on. The overbar indicates an average over spatio-temporal scales larger than those of turbulence. Evolution equations for the mean momentum and mean tracer become (Gill 1982)

$$\frac{\partial \overline{\vec{u}}}{\partial t} + \overline{\vec{u}} \cdot \nabla \overline{\vec{u}} = -\frac{1}{\rho} \nabla \overline{p} + \vec{g} - f \vec{z} \times \overline{\vec{u}} + \nabla \cdot \nu \nabla \overline{\vec{u}} - \overline{\vec{u'} \cdot \nabla \vec{u'}}, \tag{3}$$

$$\frac{\partial \overline{C}}{\partial t} + \overline{\vec{u}} \cdot \nabla \overline{C} = \overline{Q_C} + \nabla \cdot \kappa_C \nabla \overline{C} - \overline{\vec{u'} \cdot \nabla C'}. \tag{4}$$

The last terms in (3) and (4) imply that correlations between fluctuations in velocity and velocity (or tracer) gradients can modify the mean velocity (or tracer) tendency. Using the continuity equation under Boussinesq approximation $\nabla \cdot \vec{u} = 0$, and assuming turbulent fluxes can be modelled by down-gradient Fickian diffusion, the system of equations is closed with

$$\overline{\vec{u'} \cdot \nabla C'} = \nabla \cdot \overline{\vec{u'} C'} = \nabla \cdot (-\vec{K_C} \cdot \nabla \overline{C}) \tag{5}$$

and analogous relations for each component of the mean velocity vector. In (5), we introduced the (a priori unknown) turbulent diffusivity vector $\vec{K_C}$. In most oceanic conditions, each component of the turbulent diffusivity vector will exceed its molecular counterpart and molecular terms in (3) and (4) can be neglected. However, molecular processes are still necessary and operate to dissipate variance: it is via an increase of the gradients available to molecular diffusivities that stirring increases rates of irreversible mixing. The phrase *irreversible mixing* refers to mixing involving molecular interactions and diminishing the domain-wide variance, whereas *stirring* refers to a transfer of variance to smaller scales.

Equations (3)-(5) imply that the impact of mixing on mean ocean circulation depends on the magnitude of turbulent diffusivities. Key to estimating these diffusivities is an understanding of

the rate-controlling processes that transfer variance to dissipation scales. Two pivotal regimes of oceanic turbulence have been identified: three-dimensional or small-scale turbulence, and geostrophic turbulence. Three-dimensional turbulence, triggered by gravitational and shear instabilities, is active on scales of 1-100 m. It induces isotropic turbulent mixing rates that range from molecular levels to 10-100 $m^2\ s^{-1}$. Values above $10^{-2}\ m^2\ s^{-1}$ occur mostly within surface and bottom boundary layers, where boundary conditions are immediately felt (Large et al. 1994, van Haren and Gostiaux 2012). Away from boundaries, moderate turbulence levels are largely sustained by the breaking of internal waves generated by tides (Fig. 3a,b; Kunze et al. 2006, Waterhouse et al. 2014, de Lavergne et al. 2020). Three-dimensional turbulence mixes tracers and momentum alike, although the isotropic diffusivities of momentum and tracers can differ (Gaspar et al. 1990).

Geostrophic turbulence consists of mesoscale eddies, with a typical diameter of 10-100 km and a baroclinic velocity structure that spans the whole water column. Most of these eddies are generated by baroclinic instability of the large-scale flow environment (Charney 1947, Eady 1949, McWilliams and Chow 1981). As opposed to three-dimensional turbulence, they stir background tracer gradients only along density surfaces in the ocean interior (Iselin 1939, McDougall et al. 2014), and horizontally near the surface, at estimated rates varying from about 10 to $10^4\ m^2\ s^{-1}$ (Fig. 3c,d; Klocker and Abernathey 2014, Cole et al. 2015, Groeskamp et al. 2020, Chapter 9). In the surface boundary layer and where tracer surfaces are not aligned with density surfaces, mesoscale eddies are thus able to produce finescale tracer variance (Klein et al. 1998). This variance is ultimately dissipated at molecular scale with the aid of background three-dimensional turbulence (Smith and Ferrari 2009, Naveira Garabato et al. 2016). The cooperation of mesoscale, small-scale and molecular processes thus contributes to the homogenization of all tracers along density surfaces. Density surfaces being called *isopycnals*, the

phrase *isopycnal mixing* is often used as a shorthand for this suite of processes.

Rates of isopycnal mixing are thought to be set by mesoscale stirring, rather than by three-dimensional turbulence (Chapter 9). Stirring rates by mesoscale eddies are typically seven orders of magnitude larger than isotropic diffusivities. Consequently, mixing by three-dimensional turbulence is usually referred to as *diapycnal mixing*: its contribution to mixing along isopycnals being overwhelmed by that of geostrophic turbulence, only the contribution to mixing across isopycnals is considered. Because diapycnal gradients are well approximated by vertical gradients except at boundaries, diapycnal mixing is also frequently referred to as *vertical mixing*. We instead use the phrase *isotropic mixing*, for it is the most general and physical description of mixing by small-scale turbulence (McDougall et al. 2014).

In addition to tracer stirring, geostrophic turbulence causes efficient lateral and vertical redistribution of horizontal momentum (Rhines and Holland 1979). Mathematically, these effects reside in the last term of equation (3). The lateral redistribution effect, termed Reynolds stress, is often modelled by down-gradient diffusion along geopotential surfaces (Munk 1950, Smith and McWilliams 2003). However, this diffusive representation of momentum fluxes is imperfect because mesoscale eddies can transfer momentum up-gradient and accelerate or rectify the large-scale flow (Harrison 1978, Rhines and Holland 1979). The vertical redistributive effect, called eddy form stress, has a profound effect on large-scale currents (Johnson and Bryden 1989, Olbers 1998): even though mesoscale eddies are unable to flux tracers across isopycnals, they are adept at transferring momentum across isopycnals via pressure fluctuations. The induced vertical momentum transfers may be represented as Fickian vertical mixing provided the diffusivity has an appropriate form (Rhines and Young 1982, Gent et al. 1995). However, they are more commonly represented and interpreted as an eddy-induced mass transport due to cor-

relations between mesoscale velocities and isopycnal layer thicknesses (Gent and McWilliams 1990, McDougall and McIntosh 2001).

The example of eddy form stress shows that the same physical process can have alternative diffusive and advective representations, illustrating the difficulty in defining mixing. Still, it is possible to distinguish processes that unambiguously contribute to irreversible mixing, and thereby dissipate whole-ocean kinetic energy and/or tracer variance. Reynolds and eddy form stresses exerted by geostrophic turbulence do not qualify: they communicate momentum via pressure gradient forces rather than molecular friction. By contrast, three-dimensional turbulence directly contributes to dissipate both kinetic energy and tracer variance. Similarly, tracer stirring by geostrophic eddies contributes to irreversible mixing by transferring variance down to dissipation scales. In the remainder of this chapter, we will reserve the word *mixing* for only those processes causing irreversible mixing, and discuss the role of such processes in basin-scale ocean circulation (sections 4-7). In the next section, we briefly expose ocean circulation theories that do *not* appeal to mixing.

3. Non-dissipative theories of ocean circulation

In 1992, a purposeful tracer release experiment at 300 m depth in the northeastern Atlantic showed that the isotropic diffusivity in the region's pycnocline is close to 10^{-5} m^2 s^{-1} (Ledwell et al. 1993). Temperature microstructure in the stratified upper ocean indicates similar average rates of temperature mixing, despite integrating the additional contribution of geostrophic turbulence (Osborn and Cox 1972, Gregg 1987, Davis 1994). At the rate of 10^{-5} m^2 s^{-1}, diffusive heat transfer over 1 km takes about 3,000 years: too slow to compete with surface heat forcing and heat transport by upper-ocean currents. These observations motivated—or justified a

posteriori—the neglect of molecular-scale dissipation in landmark models of ocean circulation.

a. Ekman pumping

The first such model is due to Sverdrup. Classical scaling of equation (1) shows that, away from the equator, ocean currents are close to geostrophic balance: pressure gradient and Coriolis forces set horizontal velocities. Cross-differentiation of zonal and meridional geostrophic equations and use of continuity yields

$$\beta v = f \frac{\partial w}{\partial z} \tag{6}$$

where $\beta = df/dy$. Equation (6) states that poleward (equatorward) flow must be balanced by vertical stretching (squeezing) of fluid columns. Winds are a prominent force able to squeeze or stretch water columns: the curl of the surface wind stress $\vec{\tau}$ generates a pumping velocity w_{Ek} at the base of the thin surface Ekman layer. Vertical integration of (6) from a depth h_0 of assumed zero vertical motion up to the bottom of the Ekman layer (of thickness h_{Ek}) gives Sverdrup's prediction for the meridional circulation,

$$\beta \int_{z=-h_0}^{z=-h_{Ek}} v \, dz = f w_{Ek} = f \nabla \times (\vec{\tau}/f) \; . \tag{7}$$

Relation (7), called Sverdrup balance, proved very powerful to explain the broad equatorward (poleward) flow of subtropical (subpolar) gyres (Fig. 4). In this model, depth-integrated currents are shaped by direct wind forcing. This forcing relies on the existence of molecular friction, necessary for winds to transfer momentum to an initially still ocean surface. Yet wind stress effectively occurs via pressure forces onto surface waves (Plant 1982), so that Ekman pumping and Sverdrup balance do not depend on viscosity.

Sverdrup balance is mute about the vertical structure of circulation and density in the ocean.

The three-dimensional circulation problem is particularly complex because surface buoyancy fluxes, interior density gradients and ocean currents all depend upon each other. A major advance owes to Luyten et al. (1983), who established an adiabatic theory for the large-scale currents and density structure of the ocean thermocline. They assumed that the thermocline consists of a few homogeneous isopycnal layers governed by geostrophic and hydrostatic balances (thus retaining the first three terms on the right-hand side of (1)). Specifying surface densities where Ekman pumping is downward, they tracked the depth of isopycnals and the transport along isopycnals, progressing from the isopycnals' outcrop locations toward the equator. Their theory, called the ventilated thermocline theory, successfully predicts certain key features of the thermocline. It suggests that, underneath the direct influence of surface forcing, the density structure and ventilation of the upper ocean are essentially controlled by Ekman pumping—and largely independent of mixing.

An adiabatic model of circulation in the deep ocean was championed a decade later by Toggweiler and Samuels (1993, 1995, 1998). They proposed that a large proportion of dense waters that fill the ocean deeper than about 2 km are drawn to the surface by Ekman upwelling in the Southern Ocean (Fig. 5). There, westerly winds drive a divergent northward Ekman transport, while a zonally unbounded channel at Drake Passage latitudes (0-2 km; 56-60°S) results in the selection of deeper waters as the mass replacement for the surface divergence (Toggweiler and Samuels 1995). Indeed, within this channel, the zonal mean longitudinal pressure gradient is zero, and so the net meridional geostrophic flow must also be zero. Numerical experiments with global ocean models further showed that the wind-driven upwelling of dense waters occurs along rising isopycnals (Fig. 5) and persists in the limit of zero mixing (Toggweiler and Samuels 1998, Wolfe and Cessi 2011). This implies that an inter-hemispheric overturning circulation, akin to that schematized in Fig. 1b, can exist without mixing: (i) gravitational sinking

at northern high latitudes carries dense waters into the deep ocean; (ii) geostrophic southward flow brings these waters to the Ekman divergence south of 50°S, where they are lifted up to the surface; (iii) surface density transformations and northward upper-ocean currents close the circulation.

b. Momentum redistribution by geostrophic turbulence

Sverdrup balance does not explain the closure of gyres, which occurs via a return flow focused along the western boundary of ocean basins (Fig. 4). This return flow was long thought to rely on lateral Reynolds stresses induced by the mesoscale eddy field (Munk 1950, Pedlosky 1996). Form stress exerted by sloping bottom topography has more recently been acknowledged as the principal force upsetting Sverdrup balance along western boundaries (Hughes and de Cuevas 2001). Realistic ocean models indicate that both variable topography and geostrophic turbulence contribute to alter the balance (7) and shape the depth-integrated flow of major gyres (Le Corre et al. 2020). The same applies to the momentum balance of the Antarctic Circumpolar Current (ACC), the World Ocean's largest current which flows eastward in the latitude range 40-70°S (Fig. 4). There, bottom form stress due to topographic obstacles along the ACC path provides the sink of zonal momentum necessary to balance that imparted at the surface by westerly winds (Munk and Palmén 1951). In this balance, geostrophic turbulence plays an essential role by transferring momentum downward via eddy form stresses, connecting the surface source to the bottom sink of zonal momentum (Olbers 1998, Ferreira et al. 2005).

Momentum redistribution by geostrophic eddies plays a similarly essential role in the ocean's overturning circulations. Surface wind and buoyancy forcing often produces relatively steep isopycnal slopes that are baroclinically unstable. Baroclinic instability then generates mesoscale

eddies that act to flatten out the isopycnals (Gent et al. 1995). The slumping of isopycnals occurs via an eddy-induced baroclinic circulation which generally opposes Ekman pumping velocities (Marshall 1997, Marshall et al. 2002, Doddridge et al. 2016). This circulation alters the shallow overturning cells that span the subtropical thermocline (Doddridge et al. 2016) as well as the deep overturning circulation (Marshall and Speer 2012). In particular, mesoscale eddies can induce southward isopycnal mass fluxes within the zonally continuous ACC (Marshall 1997, Marshall and Radko 2003), thus overcoming the constraint on upper ocean southward flow at Drake Passage latitudes suggested by Toggweiler and Samuels (1995). Nevertheless, simulations of the Southern Ocean including realistic topography and a rich eddy field suggest only weak southward crossing of the ACC via eddy-induced mass transport (Zika et al. 2012, Mazloff et al. 2013, Dufour et al. 2015).

Lateral and vertical stresses induced by geostrophic turbulence thus modulate the ocean's response to Ekman pumping and surface buoyancy fluxes, implying a role for the ocean's chaotic nature in setting its circulation and stratification. However, the theories outlined in this section include no explicit role for temperature and salinity modification by turbulent mixing. Instead, they rationalize many of the observed features of the ocean by invoking purely adiabatic dynamics, asserting a view of ocean circulation in step with the scenarios illustrated in Fig. 1a,b.

4. How can mixing shape circulation?

a. By altering surface wind and buoyancy forcing

The conceptual frameworks exposed in the previous section take the wind stress and surface buoyancy fluxes or surface densities as given. However, these surface boundary conditions,

essential drivers of ocean circulation, depend on mixing and on the circulation itself.

First, the wind stress is a function of the difference between the wind velocity vector above the sea surface and the oceanic surface velocity vector (Pacanowski 1987, Duhaut and Straub 2006). Vertical momentum mixing near the surface acts to reduce the ocean surface velocity, generally augmenting the wind stress.

Second, surface heat and freshwater fluxes depend upon the sea surface temperature (SST), which is profoundly affected by mixing in the surface boundary layer. For example, SST cooling by surface heat loss in winter is generally damped by isotropic mixing, which redistributes the heat loss over the depth of the surface mixed layer. More generally, a given air-sea heat (or freshwater) flux induces a change in the temperature (or salinity) of the ocean surface that is inversely proportional to the mixed layer depth (MLD). Mixing processes controlling the MLD and its evolution thus play a major role in establishing surface densities and surface buoyancy fluxes. These processes include both momentum mixing (which affects the shear of Ekman and other currents, which in turn influences turbulence and MLD) and temperature and salinity mixing by mesoscale, submesoscale and three-dimensional turbulence (see Chapters 4 and 8).

b. By altering density gradients

On horizontal scales exceeding several kilometers, and away from frictional boundary layers, the ocean is in near geostrophic and hydrostatic balances. Combined, these balances give the thermal wind relationship

$$f\frac{\partial u}{\partial z} = g\frac{\partial \rho}{\partial y}, \quad f\frac{\partial v}{\partial z} = -g\frac{\partial \rho}{\partial x} \tag{8}$$

showing that the vertical variation of horizontal velocities is controlled by horizontal density

gradients. This implies that isotropic mixing can change horizontal circulation by altering horizontal variations in density. For example, localized deepening and densification of the surface mixed layer via surface buoyancy loss and convective mixing can stimulate horizontal motion around the convective chimney. On the other hand, isopycnal mixing catalyzed by mesoscale eddies does not modify density except for effects related to the non-linearity of the equation of state (McDougall 1984), and is therefore less able to modify horizontal circulation. In general, salinity and temperature modifications that have compensating effects on density have no impact on circulation unless they influence surface buoyancy forcing. Mixing of passive tracers is equally neutral to circulation—unless it impacts phytoplankton concentrations and, via their modulation of albedo and light absorption, near-surface densities (Sweeney et al. 2005).

Mixing can also affect circulation by altering the vertical density distribution. The densest ocean waters are formed at the surface by heat and freshwater loss to the atmosphere and cryosphere. Their gravitational, ageostrophic sinking into the deep ocean relies on their higher density relative to underlying waters. This density difference (between newly formed dense waters and underlying waters) owes to the mixing of sinking waters with lighter waters en-route to the deep ocean. Mixing thus maintains relatively low densities in the deep ocean that sustain the downwelling of the densest waters. As incoming dense waters intrude below older waters, they drive a compensating upwelling of these older waters. This upwelling is often quantified by a diapycnal velocity ω, related to the divergence of the mixing-driven density flux F (Nurser et al. 1999),

$$\omega = \frac{\partial F}{\partial \rho} \ . \tag{9}$$

Equation (9) states that local density loss due to a divergent density flux is balanced by upward advection of denser water—with the reverse true for a convergent density flux. The diapycnal velocity ω may be a true Eulerian velocity, as required at steady state, or merely a down-

ward (upward) movement of the isopycnal due to local lightening (densification). Note that the term diapycnal upwelling (downwelling) is used when the velocity ω is directed toward lighter (denser) layers, even though the orientation of the velocity may vary.

Vertical velocities induced by mixing can then set up horizontal circulations (Stommel 1958, Pedlosky 1992). Indeed, equation (6) shows that, if the vertical velocity varies in the vertical, meridional geostrophic flow is expected to balance the local squeezing or stretching. For example, Stommel (1958) proposed that widespread upwelling across the 2 km depth interface generates broad interior poleward motion at depths greater than 2 km. Pedlosky (1992) further demonstrated that longitudinal variations in the upwelling rate can cause the deep meridional flow to have a sheared, baroclinic structure.

c. By producing and consuming water masses

In the above situation of gravitational sinking enabled by mixing-driven reductions in density at depth, a circulation is established between the surface source and the bottom sink of dense waters. This perspective can be generalized as follows. Mixing both produces and consumes water masses; that is, it adds and removes mass from given density classes. If the ocean stratification is statistically steady, isopycnal mass transports (i.e., circulation) must connect the sources and sinks of mass within each isopycnal layer. Reciprocally, for an isopycnal circulation to be maintained, mass must be added at the starting point of the circulation and removed at its finish point. The mass gains and losses of isopycnal layers, referred to as *density transformations* or *water-mass transformations*, can occur at the surface via surface buoyancy fluxes, at the bottom via geothermal heating, or in the remainder of the ocean via mixing (Groeskamp et al. 2019).

Were mixing absent, circulation across density classes would be restricted to boundaries. This restriction is best illustrated by examining circulation in a density-depth coordinate system (Nycander et al. 2007; Fig. 6). In this space, the adiabatic circulations of Luyten et al. (1983) and Toggweiler and Samuels (1998) reduce to downward and upward motions at fixed density (Fig. 6a). They can be contrasted with the simplified overturning circulation of Munk and Wunsch (1998), whereby low-latitude upwelling from 4 to 1 km depth is enabled by mixing-driven buoyancy gain (Fig. 6b). By causing density transformations throughout the ocean volume, mixing thus confers an additional degree of freedom on the circulation. Whether observed overturning circulations are closer to the idealized scenarios of Figs. 1b and 6a, versus those of Figs. 1d and 6b, remains a matter of debate. We will argue that a more faithful depiction of the overturning involves a substantial decrease of density during the descent of dense waters, a modest decrease during their ascent along the seafloor, and upwelling at constant density from 2.5 km depth to the near surface (Fig. 6d).

5. Where is mixing most effective at shaping circulation?

The forces that set the ocean in motion (Fig. 2) and the mechanisms identified in section 4 hint at the locations where mixing is most influential on circulation: near the surface, and near the bottom. Here we briefly survey observed distributions of isotropic mixing and mesoscale stirring to substantiate this proposal. We define the near-surface region as waters shallower than the local annual maximum MLD plus 100 m, and the near-bottom region as waters lying within 500 m of the seafloor. The intervening waters will be referred to as the ocean interior. Thus defined, the ocean interior makes up 83% of the global ocean volume.

a. Isotropic mixing, from top to bottom

The canonical pycnocline isotropic diffusivity of 10^{-5} m^2 s^{-1} is usually deemed too small to be a leading-order control of circulation and tracer budgets (Ledwell et al. 1993, Davis 1994, Munk and Wunsch 1998). To evaluate this expectation, we apply a uniform mixing rate of 10^{-5} m^2 s^{-1} to the observed density distribution (Figs. 5 and 7; Gouretski and Koltermann 2004), and deduce diapycnal velocities according to equation (9). By summing these velocities along isopycnals within each ocean basin, we obtain diapycnal mass transports (Fig. 8a), measured in Sverdrups (Sv; 1 Sv $\equiv 10^6$ m^3 s^{-1}). The density measure employed from here on is the neutral density of Jackett and McDougall (1997) which does not depend on a reference pressure. The uniform 10^{-5} m^2 s^{-1} mixing rate generates a few Sv of diapycnal upwelling within the 25.5-28 kg m^{-3} density range, and a few Sv of downwelling at lower densities (Fig. 8a). Given that deep and subtropical overturning circulations are thought to carry a few tens of Sv (Ganachaud and Wunsch 2000, Lumpkin and Speer 2007), we conclude that an average diffusivity one order of magnitude larger, i.e. 10^{-4} m^2 s^{-1}, would be required to make isotropic mixing a leading-order contributor to these circulations (Munk and Wunsch 1998).

Caveats to the above conclusion include (i) the dependence of diapycnal transports on the three-dimensional distribution of density and diffusivity (a uniform diffusivity causes different transports than a varying diffusivity with the same average) and (ii) the role of diffusivity in shaping the ocean's density distribution, which was taken as given. Nevertheless, the calculation provides a useful rule of thumb: regions where isotropic mixing plays a direct and substantial role in circulation are likely to have average diffusivities close to or larger than 10^{-4} m^2 s^{-1}.

Winds and waves maintain high levels of mixing in the surface boundary layer (Chapter 4). Typically, this layer extends over a few tens to hundreds of meters, possesses quasi homogeneous properties and isotropic mixing rates in excess of 10^{-2} m^2 s^{-1} (Gaspar et al. 1990, Large et al.

1994, de Boyer Montégut et al. 2004). When the ocean surface loses buoyancy, mixing rates are further enhanced by convective instability. Convection leads to deepening and density gain of the mixed layer (Fig. 6c), and underpins much of the pronounced seasonal cycle of MLD. Together, these surface mixing processes shape global ocean circulation and stratification by modifying surface currents and wind stresses, SST and air-sea buoyancy exchanges, as well as water-mass transformation and subduction. In particular, winter convective mixing plays a primary role in setting the properties of water masses entering and establishing the ocean's permanent stratification (Iselin 1939, Stommel 1979).

Energetic three-dimensional turbulence often encroaches below the base of the mixed layer. Turbulence may be triggered by pronounced vertical shear in the mean currents, as occurs in the shallow thermocline (near 50 m depth) of the central and eastern equatorial Atlantic and Pacific (Gregg et al. 1985, Smyth and Moum 2013, Hummels et al. 2013, Chapter 10). These mixing hotspots are outstanding: the shear of large-scale and mesoscale currents below the mixed layer is generally insufficient to set off such instabilities, particularly in the more sluggish ocean interior (Wunsch 1997). Storm-induced inertial oscillations of the mixed layer produce shear and mixing at its base (Pollard et al. 1973, Price et al. 1986, Chapter 5). In addition, these oscillations often radiate internal waves able to catalyze mixing deeper down (Alford and Gregg 2001, Jing and Wu 2014). In mid-latitude oceans, a consequent wintertime increase of the average isotropic diffusivity by up to an order of magnitude is observed down to 2 km depth (Whalen et al. 2018). Nonetheless, the wintertime diffusivity averaged over a large region remains of order 10^{-5} m^2 s^{-1} (Whalen et al. 2018, Chapter 5), except in near-surface waters where the bulk of the energy supply to mixing lies (Zhai et al. 2009, Alford 2020).

Tides constitute a leading source of three-dimensional turbulence outside mixed boundary lay-

ers (Munk 1997, Waterhouse et al. 2014, de Lavergne et al. 2019, Vic et al. 2019). When tidal currents flow over uneven seafloor, they generate internal waves called *internal tides* that propagate and fuel three-dimensional turbulence throughout the global ocean (Garrett and Kunze 2007, Chapter 6). Estimated mixing rates due to internal tides vary widely in the horizontal and vertical, from 10^{-6} m^2 s^{-1} up to 10^{-2} m^2 s^{-1} in localized hotspots (Polzin et al. 1997, Rudnick et al. 2003, Waterhouse et al. 2014). They were recently mapped over the global ocean using Lagrangian tracking of internal tide energy from sources to sinks, accounting for local and remote pathways to mixing (Fig. 3a,b; de Lavergne et al. 2020). A zonal average of the thus estimated tidal diffusivity, weighted by $|\frac{\partial \rho}{\partial z}|$ so that mean values relate to density fluxes, shows a sharp increase near 2.5 km depth from order 10^{-5} m^2 s^{-1} above to order 10^{-4} m^2 s^{-1} below (Fig. 9a). The transition at 2.5 km corresponds to the typical depth to which topographic ridges rise (Fig. 7). This zonal mean distribution indicates that internal tides cannot account for average mixing rates nearing 10^{-4} m^2 s^{-1} above the depth range of major ridges. Given the broad agreement of the mapped tidal diffusivity with available observations of internal wave-driven turbulence below 400 m (de Lavergne et al. 2020), we contend that breaking internal waves are unlikely to sustain large diapycnal flows between 400 m and 2.5 km depth.

High isotropic diffusivities deeper than 2.5 km do not necessarily imply large net diapycnal upwelling. This is because these diffusivities are sufficiently concentrated near the bottom (Fig. 9a,b) that they tend to homogenize abyssal waters, rather than lighten them by draining buoyancy from the upper ocean. Indeed, close to rough or steep topography where elevated diffusivities are observed, turbulence is bottom-intensified (Toole et al. 1994, Polzin et al. 1997). As a result, the downward buoyancy flux increases toward the seafloor, except in a thin bottom layer where it must dwindle to match the bottom boundary condition (Fig. 10b; St Laurent et al. 2001, de Lavergne et al. 2016, Ferrari et al. 2016). Bottom-enhanced turbulence thus generates

a dipole of density transformation: buoyancy gain along the seafloor, and buoyancy loss immediately above (Fig. 10c; see also Chapter 7). The bottom lightening is associated with diapycnal upwelling, whereas the overlying densification implies diapycnal downwelling. Consequently, there is a substantial degree of cancellation between upwelling and downwelling that diminishes the ability of abyssal mixing to maintain a large-scale overturning circulation (de Lavergne et al. 2016, Ferrari et al. 2016, McDougall and Ferrari 2017).

The dipole of density transformation also applies to the second major source of mixing at depth: downslope or constricted ocean currents carrying dense waters over sills or through straits (Fig. 10a; Polzin et al. 1996, Bryden and Nurser 2003). In these locations, bottom-intensified turbulence draws energy from the flow itself, lightening waters hugging the seafloor while densifying and entraining overlying waters. Sills and straits host some of the largest deep-ocean turbulence levels and diffusivities (Ferron et al. 1998, MacKinnon et al. 2008, Voet et al. 2014). The induced diapycnal transports, although localized and of both signs, are responsible for step changes in bottom ocean properties (Fig. 10d) and abyssal stratification following dense water pathways (Mantyla and Reid 1983, Bryden and Nurser 2003).

b. Mesoscale stirring, from top to bottom

The near surface is where stirring by geostrophic turbulence is expected to be most efficient at shaping circulation, for four reasons. First, the competition between variance input by surface tracer fluxes and variance removal by mixing on the global scale (section 2) implies that temperature, salinity and density contrasts tend to decrease with depth. Second, mesoscale stirring rates are surface-intensified (Fig. 3c; Ferreira et al. 2005, Cole et al. 2015, Groeskamp et al. 2017, Canuto et al. 2019). Third, isopycnal stirring near the surface can modify the mixed layer

heat budget and air-sea buoyancy forcing (Guilyardi et al. 2001, Hieronymus and Nycander 2013). Last, geometry demands that eddy stirring transitions from isopycnal to along-boundary directions within diabatic boundary layers (Treguier et al. 1997, Ferrari et al. 2008, Chapter 9). Over the depth of the surface mixed layer, mesoscale eddies thus directly affect the density field via horizontal stirring (Danabasoglu et al. 2008).

Horizontal stirring by geostrophic turbulence in the surface mixed layer has an important influence on the transformation and subduction of water masses in certain regions (Robbins et al. 2000, Price 2001, Groeskamp et al. 2016), thus affecting circulation in the deeper ocean. At the very surface, mesoscale stirring exchanges water across gradients in air-sea fluxes, modulating these fluxes and the ocean heat balance without reliance on irreversible mixing, much as sketched in Fig. 1a. In practice, however, active three-dimensional turbulence colludes with surface buoyancy forcing to dissipate the density variance produced by mesoscale currents in the surface mixed layer. Horizontal stirring and isotropic mixing thus interact to shape surface water mass transformations.

Below the surface mixed layer, isopycnal mixing can also accomplish density transformations, due to the nonlinear dependence of density on temperature and pressure. There are two separate effects, cabbeling and the thermobaric effect, which arise due to the dependence of the thermal expansion coefficient on temperature and pressure, respectively (McDougall 1984). When mixing two water parcels with different temperatures, the mixed product is denser than the average of the two initial densities, a process known as cabbeling. Via this effect, isopycnal mixing can cause densification and attendant diapycnal downwelling. Thermobaricity, on the other hand, can cause both lightening and densification, and is active when water parcels move across a substantial pressure range. Hence, for isopycnal stirring to induce significant density trans-

formations, it must mix across relatively large temperature and pressure contrasts. The ACC, whose steep isopycnals coincide with strong eddy activity and contrasting water masses, is one such region. Calculations suggest that isopycnal diffusivities of order 10^3 m^2 s^{-1} are sufficient to cause 5-10 Sv of downwelling in the ACC region (Figs. 11a and 13a,b; Iudicone et al. 2008, Klocker and McDougall 2010, Nycander et al. 2015, Groeskamp et al. 2016).

At the bottom boundary, mesoscale stirring again must follow the direction of topography rather than that of isopycnals (Greatbatch and Li 2000). Since isopycnals intersect the seafloor at right angles, due to the insulating boundary condition (Wunsch 1970), mesoscale stirring must have a diapycnal component along the bottom topography. This effect, and its coupling with smaller scale turbulence in the bottom boundary layer, has received little attention to date. Whether near-bottom mesoscale diffusivities are sufficiently large to substantially alter density transformations in the deep ocean is presently unknown.

6. Some impacts on basin-scale overturning circulation

The role of mixing in basin-scale overturning circulations is discussed in this section, focusing on quantitative assessments of mixing-driven water mass transformations. We begin with the circulation of the densest ocean waters and move progressively toward lighter layers.

a. Abyssal overturning cell

Antarctic Bottom Water (AABW) is the densest global-scale water mass. It is produced around Antarctica, sinks along the Antarctic continental slope and spreads northward to fill most of the ocean deeper than 4 km (Orsi et al. 1999). The northward deepening and ultimate grounding of

density surfaces at these depths indicate that AABW becomes progressively lighter as it flows northward (Fig. 5). Once lighter than about 28.1 kg m^{-3}, it returns southward and ultimately upward in the Antarctic divergence (Toggweiler and Samuels 1993, Ganachaud and Wunsch 2000). This circulation loop is often referred to as the abyssal overturning.

What causes the lightening of AABW along its path? The first and principal cause is mixing at sills and straits (Bryden and Nurser 2003). A map of neutral density at the ocean bottom shows that the density of bottom waters decreases from 28.4 kg m^{-3} or more near Antarctica to 28.1-28.15 kg m^{-3} at the northern end of the Indian, Atlantic and Pacific basins (Fig. 10d). This decrease occurs in steps that coincide with narrow passages connecting sub-basins, implicating intense mixing within constricted or overflowing currents (Polzin et al. 1996, Orsi et al. 1999). The second major cause is bottom-intensified mixing by breaking internal waves (de Lavergne et al. 2016, Ferrari et al. 2016), principally internal tides (Ledwell et al. 2000, Vic et al. 2019, de Lavergne et al. 2020, Chapter 6). Using a realistic map of mixing fueled by internal tides (de Lavergne et al. 2020), we estimate that tidal mixing converts about 15 Sv of 28.11-28.2 kg m^{-3} waters into lighter 28.05-28.11 kg m^{-3} waters (Fig. 8b). Of this conversion, a third occurs in the Southern Ocean (south of 32°S), 6 Sv in the Indo-Pacific and 4 Sv in the Atlantic. A third primary cause of AABW lightening is geothermal heating (Adcroft et al. 2001, Emile-Geay and Madec 2009). Incorporating the contribution of geothermal heat fluxes mapped by Lucazeau (2019) into diapycnal velocities along the seafloor, we calculate that geothermal heating augments the peak diapycnal upwelling by about 7 Sv globally (Fig. 8b). The bulk of this geothermal density transformation occurs in the wide Pacific basin and is focused around 28.11 and 28.03 kg m^{-3} densities, which cover a large fraction of the North Pacific and southeastern Pacific seafloor, respectively (Fig. 10d).

These three causes of AABW lightening are not equivalent. Mixing in constrictive passages accounts for most of the overall density contrast traversed by the abyssal overturning circulation. However, its contribution to AABW lightening is restricted to densities greater than 28.15 kg m^{-3}, and is reliant on the existence of the circulation itself. The peak diapycnal upwelling, which dictates the level of meridional flow reversal and the magnitude of the circulation, occurs at lighter densities and is largely driven by breaking internal waves and geothermal heating (de Lavergne et al. 2017). Hence, tidal mixing and geothermal heating are the actual engines of the circulation: they supply potential energy to the flow, whereas overflow mixing consumes the flow's potential energy (Huang 1999, Bryden and Nurser 2003). Still, overflow mixing profoundly affects the strength of the circulation by shaping the abyssal stratification, thus modifying internal wave-driven mixing and the upwelling rates induced by geothermal buoyancy gains (Emile-Geay and Madec 2009, de Lavergne et al. 2016).

An additional difference between geothermal heating and abyssal mixing must be underlined. Geothermal heating provides a net buoyancy gain, moving water toward lighter layers only (Fig. 6c). By contrast, abyssal mixing is dominated by bottom-intensified turbulence, which causes near-compensating gains and losses of buoyancy near the bottom (Fig. 6c). This compensation limits the ability of bottom-enhanced turbulence to drive a net circulation toward lighter layers. In particular, bottom-intensified turbulence can cause net densification of a deep water mass (de Lavergne et al. 2016), even at the basin scale, as obtained here in the 28.02-28.09 kg m^{-3} density range within the Atlantic (Fig. 8b).

Geothermal heating and bottom-enhanced turbulence share one important characteristic: they cause buoyancy gain only along the seafloor. As a result, the net buoyancy gain of a density layer depends closely on its access to the ocean floor (de Lavergne et al. 2016, 2017, Holmes

et al. 2018b). In turn, access to the seafloor is strongly constrained by the ocean's geometry (Fig. 12): 85% of the seafloor area lies deeper than 2.5 km; 8% lies between 1 and 2.5 km depth. This peculiar depth distribution of the seafloor largely restricts AABW upwelling to depths greater than 2.5 km and densities greater than 28 kg m^{-3} (Figs. 7 and 8b; de Lavergne et al. 2017). Diapycnal upwelling persists between 1 and 2.5 km depth (27.5-28 kg m^{-3}), but remains relatively constant at a magnitude of a few Sv (Fig. 8b). In this depth range, seafloor area is scarce (Fig. 12), density surfaces are relatively flat at low and middle latitudes (Figs. 5 and 7) and the isotropic diffusivity is relatively uniform in the vertical (Figs. 3a and 9). Circulation thus essentially abides by the one-dimensional recipe of Munk (1966),

$$\omega(z) = K_\rho \frac{\partial^2 \rho}{\partial z^2} \Big/ \frac{\partial \rho}{\partial z} \approx \text{constant}\,, \tag{10}$$

noting that the (horizontally averaged) vertical velocity and diffusivity are an order of magnitude less than Munk originally proposed. The 1-2.5 km depth range, or equivalently the 27.5-28 kg m^{-3} neutral density range of the modern ocean, could therefore be named the "Munk regime". This regime hosts a relatively weak and weakly divergent diapycnal circulation, in contrast to the underlying "topographic regime", where circulation is shaped by basin geometry and near-bottom mixing (Fig. 12).

Would the abyssal overturning persist in the absence of mixing? The presence of geothermal heating implies that it should persist so long as dense AABW is produced around Antarctica. Everything else equal, the abyssal ocean would be expected to become very dense, almost homogeneous, and traversed by a relatively swift circulation necessary to balance the steady geothermal buoyancy gain (Emile-Geay and Madec 2009). The abyssal circulation would have a structure broadly similar to that observed—constrained by topography and wind-driven upwelling—but would cross a much smaller density range. This thought experiment suggests

589 that the primary impact of mixing along the AABW path is to reduce the density of bottom wa-
590 ters and to increase the abyssal stratification. These effects have global repercussions through-
591 out the water column.

592 *b. North Atlantic Deep Water circulation*

593 The second major source of dense water in today's ocean is situated in the subpolar North At-
594 lantic. Deep convective mixing in the Labrador Sea forms small amounts of dense water that
595 participate in regional circulation and ventilate the deep ocean, but contribute little to global
596 overturning (Pickart and Spall 2007, Lozier et al. 2019). Denser North Atlantic Deep Wa-
597 ter (NADW) overflows at the submarine ridges that connect Scotland, Iceland and Greenland
598 (Dickson and Brown 1994). This relatively salty deep water mass then traverses the whole At-
599 lantic, flows along and across the ACC and reaches the near surface at high southern latitudes
600 (Talley 2013, Tamsitt et al. 2017). A sinuous return flow in the upper ocean closes the circu-
601 lation (Gordon 1986, Talley 2013), usually referred to as the Atlantic meridional overturning
602 circulation (AMOC).

603 The pole-to-pole journey of NADW is generally conceptualized as a largely adiabatic circu-
604 lation (Toggweiler and Samuels 1998, Wolfe and Cessi 2011, Nikurashin and Vallis 2012).
605 However, observation-based tracer and mass budgets suggest that NADW undergoes substan-
606 tial mixing with overlying and underlying waters, both within and outside the Atlantic basin
607 (Talley 2013, Naveira Garabato et al. 2014). Nordic overflows are the first and primary mix-
608 ing hotspot, and cause NADW to considerably increase in volume while decreasing in density
609 (Dickson and Brown 1994, Lumpkin and Speer 2003). This reduction of NADW's density is
610 critical because the difference in density between AABW and NADW controls their respective

volumes of influence and the depth of the AMOC (Galbraith and de Lavergne 2019, Sun et al. 2020).

Mixing-driven density transformations further downstream in the Atlantic depend in large part on the depth of NADW and its proximity to rough topography. The bulk of the southward flow occurs at depths greater than 2 km between densities 28 and 28.15 kg m^{-3} (Fig. 7b; Cunningham et al. 2007, Talley 2013), while the bulk of the Atlantic seafloor area lies at depths greater than 3 km or densities above 28.05 kg m^{-3} (de Lavergne et al. 2017). A sizeable portion of NADW is thus subject to strong near-bottom diapycnal transports. In the western Atlantic south of 45°N, bottom-enhanced turbulence is expected to make NADW colder and denser on average, because AABW covers most of the seafloor and tends to monopolize buoyancy gain. The strongest mixing of NADW with denser AABW may occur within the low-latitude fracture zones that channel flow from the western to the eastern Atlantic (Polzin et al. 1996, Mercier and Speer 1998, Demidov et al. 2007). Outflow from these channels is dominated by NADW, so that NADW occupies the deep eastern Atlantic down to the bottom (Sarmiento et al. 2007, de Lavergne et al. 2017). Mixing and geothermal heating in the abyssal eastern Atlantic thus serve to convert some of the densest (> 28.11 kg m^{-3}) NADW into lighter deep water. This conversion contributes to the temperature shift of NADW transport observed across the equator (Friedrichs et al. 1994).

What is the net effect of these density transformations on NADW? Over the whole Atlantic between 32°S and 60°N, we estimate that the impact of tidal mixing is to make NADW more homogeneous: about 5 Sv of 28.07-28.11 kg m^{-3} water are produced at the expense of denser and lighter categories (Fig. 8b). We find little upwelling of NADW across the mid-depth stratification and into the northward flowing upper branch of the circulation: only about 1 Sv of

28-28.03 kg m^{-3} water is converted into < 27.6 kg m^{-3} water (Fig. 8b). The actual amount of NADW upwelling into the Atlantic pycnocline may be larger, notably due to non-tidal sources of mixing that may dominate near the basin's western boundary (Zhai et al. 2010, Clément et al. 2016). Nonetheless, presently estimated diapycnal transports back the notion that the vast majority of NADW is exported all the way to the Southern Ocean (Toggweiler and Samuels 1995, Gnanadesikan 1999, Talley 2013).

c. Southern Ocean upwelling: adiabatic or diabatic?

Deep waters flowing out of the Pacific, Indian and Atlantic basins are thought to upwell along the sloping isopycnals of the Southern Ocean (Fig. 5; Toggweiler and Samuels 1993, Marshall 1997, Sloyan and Rintoul 2001, Marshall and Speer 2012). This upwelling is generally called adiabatic in the sense that it is density preserving (see Chapter 12). However, the isopycnal flow crosses isotherms and isohalines (Zika et al. 2009, Naveira Garabato et al. 2016, Tamsitt et al. 2018). This implicates mixing, enhanced by geostrophic and small-scale turbulence, in the temperature and salinity modifications of deep waters along their isopycnal upwelling path.

Diapycnal upwelling in the ACC has been suggested to play a role in returning deep waters to the surface. The main supporting evidence comes from the observed rapid spreading of passive tracers across isopycnals in the Atlantic sector of the ACC (Naveira Garabato et al. 2007, Watson et al. 2013). Within this sector, the measured spreading rate is consistent with a mid-depth isotropic diffusivity of order 10^{-4} m^2 s^{-1}. Applied to the climatological stratification of the Southern Ocean, a uniform mixing rate of this magnitude would cause about 10 Sv of diapycnal upwelling south of 32°S (Fig. 8a). However, the actual diapycnal flow is most certainly only a fraction of this rate, because diapycnal tracer spreading is slower in less hilly

sectors of the ACC (Ledwell et al. 2011, Watson et al. 2013), and because the effective mixing rate of a passive tracer can far exceed the effective mixing of density (Mashayek et al. 2017). Indeed, passive tracers tend to hover in regions of weak flow, elevated mixing and reduced stratification near topographic obstacles (Mashayek et al. 2017). Microstructure observations of turbulence in the Scotia Sea suggest that the effective mixing rate of density is much weaker than the diffusivity inferred from passive tracer measurements (St Laurent et al. 2012, Sheen et al. 2013).

Diapycnal downwelling of deep waters is equally plausible. Observations indicate that energetic turbulence in the ACC is often bottom-intensified. If dominated by bottom-enhanced turbulence, isotropic mixing could cause a few Sv of net diapycnal downwelling of circumpolar deep waters (Melet et al. 2014, de Lavergne et al. 2016). Estimated diapycnal transports due to tidal mixing south of 32°S indicate that upwelling dominates but remains weak at densities less than 28.05 kg m^{-3} (Fig. 8b). Net diapycnal downwelling may also arise from isopycnal mixing and the non-linearity of the equation of state (Iudicone et al. 2008, Klocker and McDougall 2010, Groeskamp et al. 2016). We estimate that cabbeling and thermobaricity combined cause diapycnal downwelling varying between 2 and 4 Sv at densities larger than 27.5 kg m^{-3} in the Southern Ocean (Fig. 11b). This downwelling may act to shift the upwelling toward larger densities or to increase the northward flow of AABW.

Hence, net diapycnal flow of deep waters in the ACC is most likely an order of magnitude weaker than the overall upwelling rate, thought to be between 20 and 30 Sv (Lumpkin and Speer 2007, Naveira Garabato et al. 2014). Upwelling does become diapycnal near the surface, however: alongside surface buoyancy forcing, mixing by three-dimensional turbulence plays an essential role in the entrainment of deep waters into the surface mixed layer and the diabatic

closure of the Southern Ocean overturning (Gordon and Huber 1990, Iudicone et al. 2008, Abernathey et al. 2016, Evans et al. 2018).

d. The return flow to the North Atlantic

NADW formation is the conversion of about 15 Sv of water from the ventilated pycnocline (densities < 27.5 kg m^{-3}) into denser waters (Lumpkin and Speer 2003). The compensating conversion can occur either through mixing-driven upwelling at low and middle latitudes (Munk and Wunsch 1998) or through near-surface lightening in the Southern Ocean (Toggweiler and Samuels 1993). We estimate that isotropic mixing causes about 3 Sv of upwelling across the 27.5 kg m^{-3} isopycnal (Figs. 8b and 13c), while isopycnal mixing induces an opposite transport of similar magnitude (Figs. 11b and 13a,b). These estimates imply that the net mass gain of the ventilated pycnocline occurs almost exclusively near the surface at southern high latitudes (Gnanadesikan 1999). A return flow of about 15 Sv must therefore exist from the Antarctic source of light water (< 27.5 kg m^{-3}) to its sink in the northern North Atlantic.

The first stage of this return route is the formation of mode and intermediate waters on the northern side of the ACC. Mixing in the surface boundary layer and immediately below plays an essential role in the formation of these subantarctic waters (McCartney 1977, Sloyan and Rintoul 2001, Iudicone et al. 2008, Sloyan et al. 2010). Cabbeling has also been highlighted as an important contributor to the formation of intermediate waters (Urakawa and Hasumi 2012, Nycander et al. 2015, Groeskamp et al. 2016). Along the northern flank of the ACC, cold and fresh southern waters come close to warmer and saltier subtropical waters within an active mesoscale eddy field (Abernathey et al. 2010). We estimate that the resultant mixing along isopycnals forms about 2 Sv of intermediate water in the 27.25-27.5 kg m^{-3} range (Figs. 11b and

13a,b). This number is somewhat lower than previous estimates. We attribute the difference primarily to the suppression of mesoscale stirring by mean currents (Ferrari and Nikurashin 2010). This suppression effect, included in the employed map of mesoscale diffusivities (Groeskamp et al. 2020), limits the intensity of isopycnal mixing and associated density transformations in the upper kilometer of the ACC (Fig. 3c).

A large fraction of subducted subantarctic waters feeds the return branch of the AMOC (Schmitz 1995). In the subtropical North Atlantic, this return branch is dominated by near-surface waters that are about 15°C warmer than subantarctic waters (Schmitz and Richardson 1991). This implies that substantial warming and lightening must occur along the journey (Fig. 5). Inverse box models suggest that the bulk of this transformation occurs at low latitudes in the eastern Pacific and Atlantic and relies largely on isotropic mixing (Lumpkin and Speer 2003, Sloyan et al. 2003). Elevated mixing in the upper layers of the eastern equatorial Pacific could be an important contributor to diapycnal upwelling of subantarctic water (Gregg et al. 1985, Smyth and Moum 2013, Holmes et al. 2018a). However, it remains unclear whether observed mixing is sufficient to accommodate the required cold to warm conversion. Toggweiler et al. (2019a,b) hypothesize that most of the conversion is actually achieved by direct atmospheric forcing near eastern margins. They propose that the AMOC indirectly draws warm water westward in the Pacific and Atlantic, exposing cool subantarctic water to surface heating at the eastern end of the basins. Their mechanism is well illustrated by the schematic of Fig. 1b (equating the cold water exposed to heating in the south with subantarctic water exposed at eastern margins) and alleviates the requirement for strong low-latitude mixing beneath and across the thermocline.

e. Shallow hemispheric cells

In addition to the return branch of the AMOC, the upper ocean hosts several closed overturning cells. The most prominent cells inhabit the top few hundred meters of subtropical oceans. These subtropical cells involve subduction poleward of about 20° and upwelling near the equator, connected by poleward surface Ekman flow and equatorward subsurface geostrophic flow (Roemmich 1983, Luyten et al. 1983, McCreary and Lu 1994, McPhaden and Zhang 2002). Convective mixing due to surface buoyancy loss shapes the rates and patterns of subduction (Marshall and Nurser 1991, McCreary and Lu 1994, Qu et al. 2013), while shear-driven mixing above the equatorial undercurrent in the Pacific and Atlantic contributes to lighten and return to the surface the upwelling waters (Lu et al. 1998, Moum et al. 2009, Hummels et al. 2013). Overall, subsurface isotropic mixing plays a key role in regulating the net overturning transport, that is, the residual of opposing Ekman and eddy-driven circulations (Henning and Vallis 2004, Doddridge et al. 2016).

Perhaps more importantly, climate model experiments have shown that SSTs, MLDs and the vertical structure of the thermocline are sensitive to the representation of isotropic mixing rates in the low-latitude upper ocean (Jochum et al. 2013, Melet et al. 2016, Zhu and Zhang 2019, Hieronymus et al. 2019, Chapter 2). Mixing near the surface has a weighty influence on air-sea interactions (Moum et al. 2013, Jochum et al. 2013, Zhu and Zhang 2019), while mixing in the interior affects the heat content of the thermocline and heat transport by the AMOC (Melet et al. 2016, Holmes et al. 2019, Hieronymus et al. 2019). Hence, the direct impacts of mixing on the ocean's temperature distribution have ripple-like effects on circulation within the thermocline and beyond.

7. Some impacts on basin-scale horizontal circulation

We define horizontal circulations as networks of zonal and meridional currents integrated over a chosen depth range. An overturning circulation generally has a signature in horizontal circulation: for example, the Gulf Stream participates in both the AMOC and in the North Atlantic gyre circulation. The impacts outlined in the previous section thus have counterparts for circulation in the horizontal plane. We expand below on the consequences of mixing for the large-scale horizontal flow of the upper ocean, the abyss and the ACC.

a. Upper-ocean gyres

Sverdrup balance (7) suggests that depth-integrated flow is controlled by the wind stress curl. Munk (1950) first tested this prediction using observed winds. He introduced an additional Reynolds stress term (able to accommodate concentrated boundary currents) and showed that the main wind patterns create cyclonic subpolar gyres and anticyclonic subtropical gyres that resemble observed upper-ocean currents. This finding demonstrated that Ekman pumping is a major determinant of gyre circulations in upper layers of the global ocean. It was a sign that other factors, such as buoyancy forcing and mixing, are less important.

When applying (7), Munk (1950) assumed that vertical motion vanishes near 1 km depth, so that squeezing and stretching of the ocean's top kilometer is set by Ekman pumping velocities at the base of the Ekman layer. Could deep vertical motion sustained by mixing and overturning alter the rates of squeezing and stretching that shape upper-ocean gyres? Ekman pumping velocities are of order 10^{-6} m s^{-1} or 30 m per year (Roquet et al. 2011). In Fig. 13, we map the velocity across the 27.5 kg m^{-3} isopycnal that is necessary to balance estimated mixing-driven density transformations. Diapycnal velocities reach values of order 10^{-6} m s^{-1} only in specific hotspots of water mass transformation or near the outcropping or incropping of the considered isopycnal.

Over the vast majority of the upper ocean, Ekman pumping is therefore expected to dominate, suggesting that mesoscale stirring and tidal mixing play only a small role in driving gyres via squeezing and stretching of the ventilated pycnocline.

Regional hotspots of water mass transformation can nonetheless have major local and remote impacts on upper-ocean gyres, mediated by changes in regional density structure and mass balance. For example, mixing in the Nordic overflows has a first-order influence on the horizontal upper-ocean circulation of the whole North Atlantic (Lumpkin and Speer 2003, Zhang et al. 2011). Large tidal mixing rates in the western Pacific and Indonesian archipelago impact the throughflow between—and the gyres within—Pacific and Indian basins (Koch-Larrouy et al. 2010, Sasaki et al. 2018). In general, impacts of mixing on the AMOC have repercussions for the basin-scale horizontal circulation of the upper ocean (Toggweiler et al. 2019b).

Mixing near the surface plays a direct and widespread role. Subtropical gyres are linked to subtropical overturning cells (McCreary and Lu 1994, Samelson and Vallis 1997) and are therefore influenced by near-surface mixing via the mechanisms described in section 6e. Subpolar gyres conform less to Sverdrup balance than their subtropical twins: they are more strongly influenced by nonlinear dynamics and surface buoyancy forcing (Bryan et al. 1995, Su et al. 2014, Le Corre et al. 2020). In the Southern Hemisphere, near-surface meridional density gradients are the leading control on the strength of subpolar gyres simulated by climate models (Wang and Meredith 2008). These gradients, primarily set by freshwater and heat exchanges with the atmosphere and cryosphere, are modulated by mixing (Pellichero et al. 2017, Thompson et al. 2018).

b. The Stommel and Arons circulation

Horizontal circulation patterns in the deep ocean have received comparatively little attention. The reference theory for these patterns was proposed sixty years ago by Stommel (1958) and Stommel and Arons (1959a,b). This theory is based on equation (6) integrated from the seafloor ($z = -H$) to a chosen abyssal depth ($z = -h_{top}$):

$$\beta \int_{z=-H}^{z=-h_{top}} v \, dz = f[w(z = -h_{top}) - w(z = -H)] \, . \tag{11}$$

Stommel (1958) reasoned that the production and sinking of cold waters near Greenland and Antarctica should be balanced by downward diffusion of heat and upwelling across stratification at lower latitudes. Using (11) and assuming that the upwelling velocity at 2 km depth exceeds that at the bottom, Stommel mapped mass transports below 2 km as broadly poleward except near western boundaries, where fast currents governed by different dynamics were assumed to close the mass balance.

The circulation patterns drawn by Stommel (1958) and Stommel and Arons (1959a,b) have been shown to hold in idealized flat-bottom model oceans where a deep overturning is maintained by downward diffusion of buoyancy at a uniform rate (Samelson and Vallis 1997). Observational inferences of deep circulation have invariably revealed a different and much more complex picture (Friedrichs and Hall 1993, Hautala and Riser 1993, Reid 1997, 2003). Reasons are manifold. First, the theory assumes that the deep ocean hosts divergent vertical motion everywhere away from sinking regions. In reality, the area-integrated upwelling rate of deep waters at low and middle latitudes increases with height only up to about 4 km depth, then decreases with height until about 2.5 km depth (Fig. 8b; de Lavergne et al. 2017). Meanwhile, the ocean area increases markedly, so that the area-averaged upwelling tends to be less divergent than its area-integrated counterpart (McDougall 1989, Rhines 1993). Hence, convergent vertical motion favoring equatorward flow may be more common than the reverse. Moreover, upwelling

is not horizontally uniform: it is a balance of upward and downward velocities that are largest near topography (Fig. 10). Bottom-intensified mixing entails complex patterns of squeezing and stretching that depend on local characteristics of topography and turbulence (St Laurent et al. 2001, McDougall and Ferrari 2017).

More importantly, horizontal flow in the abyss is strongly constrained by topography and is influenced by a range of dynamics not reflected in the combination of (9) and (11) (Holland 1978, Garrett 1991, Pedlosky 1992, Callies 2018, Naveira Garabato et al. 2019, Yang et al. 2020; see also Chapters 7 and 8). How mixing interacts with such dynamics to shape abyssal current systems is expected to vary between regions and remains little studied.

c. The Antarctic Circumpolar Current

The ACC transports over 130 Sv eastward as it circumnavigates Antarctica (Fig. 4; Meredith et al. 2011). The current has its largest speeds at the surface, but extends down to the seafloor (Peña-Molino et al. 2014). It is deemed to be driven in large part by Southern Hemisphere westerly winds (Munday et al. 2011, Howard et al. 2014). Indeed, if the global ocean were mixed to a single temperature and salinity, a full-depth ACC would likely persist as a conduit between momentum input at the surface and removal into the solid earth.

Strong contrasts in temperature, salinity and density are actually observed across the ACC. The zonal mass transport of the ACC can therefore be decomposed into a depth-independent component equal to the bottom velocity and a depth-dependent component obtained by vertical integration of the thermal current shear (8). This second component is directly linked to the meridional density difference across the ACC and accounts for about 85% of the total eastward

transport (Peña-Molino et al. 2014). Any impact of mixing on meridional density gradients in the Southern Ocean thus has implications for the strength and vertical structure of the ACC.

For instance, larger background rates of isotropic mixing tend to lower isopycnals north of the ACC and thereby increase the thermal current shear and ACC transport (Munday et al. 2011). Likewise, deep convective mixing south of the ACC can enhance the north-south density gradient and accelerate the ACC (Behrens et al. 2016). Bottom-intensified mixing in the abyss has also been found to alter the ACC density structure and flow, in ways that depend on the latitudinal distribution of that mixing (Jayne 2009, Melet et al. 2014).

Isopycnal mixing may also affect the ACC strength. Diapycnal downwelling due to cabbeling and thermobaricity, by acting as a sink of volume for the ventilated pycnocline, could contribute to raising isopycnals north of the ACC and slowing the circumpolar flow. Furthermore, isopycnal mixing can alter air-sea interactions at high latitudes and, via the induced changes in wind stress, convection and stratification, modify the ACC (Ragen et al. 2020).

Mixing can further influence the ACC by changing the strength of the meridional overturning circulation, without necessarily changing meridional density gradients within the current. Indeed, cross-stream flows affect the zonal momentum balance of the ACC (Gent et al. 2001, Howard et al. 2014, Stewart and Hogg 2017). In particular, an increased abyssal overturning strength (such as may result from increased deep mixing) has the potential to accelerate the ACC as follows: the Coriolis force acts to deflect the northward AABW flow to the west, and the southward return flow to the east; the westward abyssal momentum is damped by topographic form stress and bottom friction; a net gain of depth-integrated eastward momentum ensues (Howard et al. 2014).

The vertical and zonal extent of the ACC makes it a crossroads of global ocean circulation (Rintoul and Naveira Garabato 2013, Chapter 12). The ACC's structure and intensity are consequently tied to water mass transformations in all parts of the World Ocean.

8. Conclusions

Munk (1966) first conjectured that mixing between water masses occurs mostly where these water masses meet the surface and the seafloor. Here we estimated that isotropic and isopycnal mixing in the ocean interior (defined as in section 5) gives rise to diapycnal circulations of only a few Sverdrups. Rates of basin-scale overturning are thought to be an order of magnitude larger (Ganachaud and Wunsch 2000, Lumkpin and Speer 2007). This implies that Munk was right, and the diapycnal component of global ocean circulation is largely confined to near-surface and near-bottom regions. Although this notion is long established (Munk and Wunsch 1998, Wunsch and Ferrari 2004), its consequences for the structure of ocean circulation remain under-appreciated.

The first and foremost consequence of boundary-intensified mixing is the organization of circulation by outcrop and incrop areas—that is, by the access of water masses to boundary regions. Three main regimes can be identified (Fig. 12): (i) a ventilated pycnocline where air-sea exchanges and mixing near surface outcrops govern the structure and rate of circulation; (ii) a topographic regime where abundant seafloor deeper than 2.5 km leads to substantial near-bottom density transformations; and (iii) an intervening Munk regime, more isolated from boundaries, where interior mixing maintains a modest diapycnal circulation. In the topographic regime, circulation is both strong and strongly influenced by near-bottom mixing. In the Munk regime, basin-averaged circulation and isotropic mixing rates are relatively weak (Figs. 7-9). In the ven-

tilated pycnocline, circulation is strong and strongly influenced by mixing near the surface, yet largely along-isopycnal in the interior.

A related consequence is the relationship between seafloor geometry and overturning circulation. Munk and Wunsch (1998), in their calculation of the effective diffusivity needed to upwell dense waters from 4 km to 1 km depth, did not account for the change with depth of the ocean's area. Actually, the small change of the ocean's area between 1 and 2.5 km depth impedes near-boundary diapycnal upwelling, whereas its rapid decrease at greater depths allows large diapycnal transports (de Lavergne et al. 2017). The depth distribution of the seafloor thus places a primary constraint on the structure of the overturning circulation. The compartmentalization of the deep ocean into subbasins connected by sills and straits exerts an additional and essential constraint (Bryden and Nurser 2003). A third crucial geometric ingredient is the interruption of north-south continental barriers in the Southern Ocean, which favours deep southward flow across the ACC (Toggweiler and Samuels 1995). Combined, these three ingredients lead to the simplified depiction in density-depth space of a bathymetrically constrained overturning (Fig. 6d).

Both NADW and AABW undergo larger density losses during their descent than their ascent, and both benefit from isopycnal Southern Ocean upwelling to come back to the surface (Fig. 6d). Differences between the abyssal overturning cell and the AMOC do nevertheless exist. The abyssal overturning cell inhabits the topographic regime and can be considered essentially diabatic, in that its existence relies on the lightening of AABW at depth (Nikurashin and Vallis 2012). NADW is partially embedded in the topographic regime and undergoes substantial transformation by near-bottom mixing (section 6b). However, density losses that are essential to the closure of the AMOC are believed to occur near the surface at southern high latitudes (Tog-

gweiler and Samuels 1998, Marshall and Speer 2012) and at low latitudes (Toggweiler et al. 2019a,b). The AMOC may thus be considered as more adiabatic, insofar as its existence and structure depend less on mixing below the near-surface region.

We posited that mixing in the ocean interior has less of an influence on circulation than near-boundary mixing, because it causes comparatively weak diapycnal flows. However, interior mixing does impact circulation in several indirect and important ways. In particular, isopycnal mixing catalyzed by mesoscale eddies modifies the temperature and salinity of water masses within the ocean interior. These modifications then affect air-sea interactions where the modified water masses outcrop (Guilyardi et al. 2001, Hieronymus and Nycander 2013, Ragen et al. 2020). In addition, weak rates of isotropic mixing in the voluminous ocean interior exert an important influence on the stratification and heat balance of the upper ocean (Melet et al. 2016, Holmes et al. 2018a, Hieronymus et al. 2019). Altered density and temperature distributions then impact the structure and strength of horizontal and overturning circulations (Sasaki et al. 2018, Zhu and Zhang 2019).

Mixing in the ocean interior is also essential for ventilation—that is, for the circulation of tracers (rather than the circulation of mass, which is the subject of this chapter). Tracer distributions are influenced by mixing via the impacts of mixing on ocean currents, but they are also directly impacted by mixing. These direct impacts are tracer specific, since diffusive tracer fluxes depend on tracer gradients in addition to diffusivities. For example, small isotropic diffusivities can cause weak buoyancy fluxes but large tracer fluxes. Weak mixing rates in the ocean interior can thus maintain important diapycnal tracer fluxes even in the absence of a diapycnal circulation. Furthermore, isopycnal mixing in the interior plays a key role in shaping global tracer distributions (Ledwell et al. 1998, Jones and Abernathey 2019) and is able to dominate over

ventilation by the large-scale mean currents (Holzer and Primeau 2006, Naveira Garabato et al. 2017). As such, interior mixing participates in setting the global state of climate and marine ecosystems in multiple and often underrated ways.

Understanding how circulation and mixing together establish the pathways and timescales of ocean ventilation constitutes a major and central challenge to this day. The recent advent of global three-dimensional maps of isotropic and isopycnal diffusivities (Fig. 3) opens up avenues for headway. However, these maps are incomplete and insufficiently constrained. New field measurements, coupled with research into the physics and energetics of turbulence across scales, are called for to incorporate all leading-order processes into comprehensive and realistic maps. Mechanistic understanding of the energy routes from forcing to circulation to mixing is essential to construct models that not only capture the observed mixing distributions, but also evolve these distributions consistently with changing boundary conditions (Eden et al. 2014). The path to faithful, conservative representation of the energy cycle (Fig. 2) in ocean models is long but vital to confidently probe and project ocean ventilation and its role in the climate system.

References

Abernathey, R., Marshall, J., Mazloff, M., Shuckburgh, E., 2010. Enhancement of mesoscale eddy stirring at steering levels in the Southern Ocean. J. Phys. Oceanogr. 40, 170–184.

Abernathey, R.P., Cerovecki, I., Holland, P.R., Newsom, E., Mazloff, M., Talley, L.D., 2016. Water-mass transformation by sea ice in the upper branch of the Southern Ocean overturning. Nature Geoscience 9, 596–601.

Adcroft, A., Scott, J.R., Marotzke, J., 2001. Impact of geothermal heating on the global ocean circulation. Geophysical Research Letters 28, 1735–1738.

945 Alford, M.H., Gregg, M.C., 2001. Near-inertial mixing: Modulation of shear, strain and mi-
946 crostructure at low latitude. J. Geophys. Res. 106, 16947–16968.
947 Alford, M.H., 2020. Revisiting near-inertial wind-work: Slab models, relative stress, and mixed
948 layer deepening. J. Phys. Oceanogr. 50, 3141-3156.
949 Behrens, E., Rickard, G., Morgenstern, O., Martin, T., Osprey, A., Joshi, M., 2016. Southern
950 Ocean deep convection in global climate models: A driver for variability of subpolar gyres
951 and Drake Passage transport on decadal timescales. J. Geophys. Res. 121, 3905–3925.
952 Bessières, L., Madec, G., Lyard, F., 2008. Global tidal residual mean circulation: Does it affect
953 a climate OGCM? Geophysical Research Letters 35, L03609.
954 Bryan, F.O., Böning, C.W., Holland, W.R., 1995. On the midlatitude circulation in a high-
955 resolution model of the North Atlantic. J. Phys. Oceanogr. 25, 289–305.
956 Bryden, H.L., Nurser, A.J.G., 2003. Effects of strait mixing on ocean stratification. J. Phys.
957 Oceanogr. 33, 1870–1872.
958 Callies, J., 2018. Restratification of abyssal mixing layers by submesoscale baroclinic eddies.
959 J. Phys. Oceanogr. 48, 1995-2010.
960 Canuto, V.M., Cheng, Y., Howard, A.M., Dubovikov, M.S., 2019. Three-Dimensional, space-
961 dependent mesoscale diffusivity: Derivation and implications. J. Phys. Oceanogr. 49,
962 1055–1074.
963 Charney, J.G., 1947. The dynamics of long waves in a baroclinic westerly current. J. Meteor.
964 4, 136–162.
965 Clément, L., Frajka-Williams, E., Sheen, K.L., Brearley, J.A., Naveira Garabato, A.C., 2016.
966 Generation of internal waves by eddies impinging on the western boundary of the North
967 Atlantic. J. Phys. Oceanogr. 46, 1067–1079.
968 Cole, S.T., Wortham, C., Kunze, E., Owens, W.B., 2015. Eddy stirring and horizontal diffusiv-
969 ity from Argo float observations: Geographic and depth variability. Geophysical Research

970 Letters 42, 3989–3997.

971 Cunningham, S.A., Kanzow, T., Rayner, D., Baringer, M.O., Johns, W.E., Marotzke, J., Long-
972 worth, H.R., Grant, E.M., Hirschi, J.J.-M., Beal, L.M., Meinen, C.S., Bryden, H.L., 2007.
973 Temporal variability of the Atlantic meridional overturning circulation at 26.5°N. Science
974 317, 935–938.

975 Danabasoglu, G., Ferrari, R., McWilliams, J.C., 2008. Sensitivity of an ocean general circula-
976 tion model to a parameterization of near-surface eddy fluxes. J. Climate 21, 1192–1208.

977 Davis, R.E., 1994. Diapycnal mixing in the ocean: The Osborn–Cox Model. J. Phys. Oceanogr.
978 24, 2560–2576.

979 de Boyer Montégut, C., Madec, G., Fischer, A.S., Lazar, A., Iudicone, D., 2004. Mixed layer
980 depth over the global ocean: An examination of profile data and a profile-based climatology.
981 J. Geophys. Res. 109, C12003.

982 de Lavergne, C., Falahat, S., Madec, G., Roquet, F., Nycander, J., Vic, C., 2019. Toward global
983 maps of internal tide energy sinks. Ocean Modelling 137, 52–75.

984 de Lavergne, C., Madec, G., Le Sommer, J., Nurser, A.J.G., Naveira Garabato, A.C., 2016. On
985 the consumption of Antarctic Bottom Water in the abyssal ocean. J. Phys. Oceanogr. 46,
986 635–661.

987 de Lavergne, C., Madec, G., Roquet, F., Holmes, R.M., McDougall, T.J., 2017. Abyssal ocean
988 overturning shaped by seafloor distribution. Nature 551, 181–186.

989 de Lavergne, C., Vic, C., Madec, G., Roquet, F., Waterhouse, A.F., Whalen, C.B., Cuypers, Y.,
990 BouruetAubertot, P., Ferron, B., Hibiya, T., 2020. A parameterization of local and remote
991 tidal mixing. Journal of Advances in Modeling Earth Systems 12, e2020MS002065.

992 Demidov, A.N., Dobrolyubov, S.A., Morozov, E.G., Tarakanov, R.Y., 2007. Transport of bot-
993 tom waters through the Vema Fracture Zone in the Mid-Atlantic ridge. Dokl. Earth Sc. 416,
994 1120–1124.

995 Dickson, R.R., Brown, J., 1994. The production of North Atlantic Deep Water: Sources, rates,
996 and pathways. J. Geophys. Res. 99, 12319–12341.
997 Doddridge, E.W., Marshall, D.P., Hogg, A.McC., 2016. Eddy cancellation of the Ekman cell in
998 subtropical gyres. J. Phys. Oceanogr. 46, 2995–3010.
999 Dufour, C.O., Griffies, S.M., de Souza, G.F., Frenger, I., Morrison, A.K., Palter, J.B., Sarmiento,
1000 J.L., Galbraith, E.D., Dunne, J.P., Anderson, W.G., Slater, R.D., 2015. Role of mesoscale
1001 eddies in cross-frontal transport of heat and biogeochemical tracers in the Southern Ocean. J.
1002 Phys. Oceanogr. 45, 3057–3081.
1003 Duhaut, T.H.A., Straub, D.N., 2006. Wind stress dependence on ocean surface velocity: Impli-
1004 cations for mechanical energy input to ocean circulation. J. Phys. Oceanogr. 36, 202–211.
1005 Eady, E.T., 1949. Long waves and cyclone waves. Tellus 1, 33–52.
1006 Eden, C., Czeschel, L., Olbers, D., 2014. Toward energetically consistent ocean models. J.
1007 Phys. Oceanogr. 44, 3160-3184.
1008 Emile-Geay, J., Madec, G., 2009. Geothermal heating, diapycnal mixing and the abyssal circu-
1009 lation. Ocean Science 5, 203–217.
1010 Evans, D.G., Zika, J.D., Garabato, A.C.N., Nurser, A.J.G., 2018. The cold transit of Southern
1011 Ocean upwelling. Geophysical Research Letters 45, 13386-13395.
1012 Ferrari, R., Mashayek, A., McDougall, T.J., Nikurashin, M., Campin, J.-M., 2016. Turning
1013 ocean mixing upside down. J. Phys. Oceanogr. 46, 2239–2261.
1014 Ferrari, R., McWilliams, J.C., Canuto, V.M., Dubovikov, M., 2008. Parameterization of eddy
1015 fluxes near oceanic boundaries. J. Climate 21, 2770–2789.
1016 Ferrari, R., Nikurashin, M., 2010. Suppression of eddy diffusivity across jets in the Southern
1017 Ocean. J. Phys. Oceanogr. 40, 1501–1519.
1018 Ferreira, D., Marshall, J., Heimbach, P., 2005. Estimating eddy stresses by fitting dynam-
1019 ics to observations using a residual-mean ocean circulation model and its adjoint. J. Phys.

Oceanogr. 35, 1891–1910.

Ferron, B., Mercier, H., Speer, K., Gargett, A., Polzin, K., 1998. Mixing in the Romanche fracture zone. J. Phys. Oceanogr. 28, 1929–1945.

Friedrichs, M.A.M., Hall, M.M., 1993. Deep circulation in the tropical North Atlantic. Journal of Marine Research 51, 697–736.

Friedrichs, M.A.M., McCartney, M.S., Hall, M.M., 1994. Hemispheric asymmetry of deep water transport modes in the western Atlantic. J. Geophys. Res. 99, 25165–25179.

Galbraith, E., de Lavergne, C., 2019. Response of a comprehensive climate model to a broad range of external forcings: relevance for deep ocean ventilation and the development of late Cenozoic ice ages. Climate Dynamics 52, 653–679.

Ganachaud, A., Wunsch, C., 2000. Improved estimates of global ocean circulation, heat transport and mixing from hydrographic data. Nature 408, 453–457.

Gargett, A.E., Osborn, T.R., 1981. Small-scale shear measurements during the fine and microstructure experiment (Fame). J. Geophys. Res. 86, 1929–1944.

Garrett, C., 1991. Marginal mixing theories. Atmosphere-Ocean 29, 313–339.

Garrett, C., Kunze, E., 2007. Internal tide generation in the deep ocean. Annual Review of Fluid Mechanics 39, 57–87.

Gaspar, P., Grégoris, Y., Lefevre, J.-M., 1990. A simple eddy kinetic energy model for simulations of the oceanic vertical mixing: Tests at station Papa and Long-Term Upper Ocean Study site. J. Geophys. Res. 95, 16179–16193.

Gent, P.R., Large, W.G., Bryan, F.O., 2001. What sets the mean transport through Drake Passage? J. Geophys. Res. 106, 2693–2712.

Gent, P.R., Mcwilliams, J.C., 1990. Isopycnal mixing in ocean circulation models. J. Phys. Oceanogr. 20, 150–155.

Gent, P.R., Willebrand, J., McDougall, T.J., McWilliams, J.C., 1995. Parameterizing eddy-

induced tracer transports in ocean circulation models. J. Phys. Oceanogr. 25, 463–474.

Gill, A.E., 1982. Atmosphere–Ocean Dynamics. Elsevier.

Gnanadesikan, A., 1999. A simple predictive model for the structure of the oceanic pycnocline. Science 283, 2077–2079.

Gordon, A.L., 1986. Interocean exchange of thermocline water. J. Geophys. Res. 91, 5037–5046.

Gordon, A.L., Huber, B.A., 1990. Southern ocean winter mixed layer. J. Geophys. Res. 95, 11655.

Gouretski, V., Koltermann, K.P., 2004. WOCE Global Hydrographic Climatology. Berichte des BSH 35, 1–52.

Greatbatch, R.J., Li, G., 2000. Alongslope mean flow and an associated upslope bolus flux of tracer in a parameterization of mesoscale turbulence. Deep Sea Research 47, 709–735.

Gregg, M.C., 1987. Diapycnal mixing in the thermocline: A review. J. Geophys. Res. 92, 5249.

Gregg, M.C., Peters, H., Wesson, J.C., Oakey, N.S., Shay, T.J., 1985. Intensive measurements of turbulence and shear in the equatorial undercurrent. Nature 318, 140–144.

Groeskamp, S., Abernathey, R.P., Klocker, A., 2016. Water mass transformation by cabbeling and thermobaricity. Geophysical Research Letters 43, 2016GL070860.

Groeskamp, S., Sloyan, B.M., Zika, J.D., McDougall, T.J., 2017. Mixing inferred from an ocean climatology and surface fluxes. J. Phys. Oceanogr. 47, 667–687.

Groeskamp, S., Griffies, S.M., Iudicone, D., Marsh, R., Nurser, A.J.G., Zika, J.D., 2019. The water mass transformation framework for ocean physics and biogeochemistry. Annual Review of Marine Science 11, 271-305.

Groeskamp, S., LaCasce, J.H., McDougall, T.J., Rogé, M., 2020. Full-depth global estimates of ocean mesoscale eddy mixing from observations and theory. Geophysical Research Letters 47, e2020GL089425.

Guilyardi, E., Madec, G., Terray, L., 2001. The role of lateral ocean physics in the upper ocean thermal balance of a coupled ocean-atmosphere GCM. Climate Dynamics 17, 589–599.

Harrison, D.E., 1978. On the diffusion parameterization of mesoscale eddy effects from a numerical ocean experiment. J. Phys. Oceanogr. 8, 913–918.

Hautala, S.L., Riser, S.C., 1993. A nonconservative β-spiral determination of the deep circulation in the eastern South Pacific. J. Phys. Oceanogr. 23, 1975–2000.

Henning, C.C., Vallis, G.K., 2004. The effects of mesoscale eddies on the main subtropical thermocline. J. Phys. Oceanogr. 34, 2428–2443.

Hieronymus, M., Nycander, J., 2013. The budgets of heat and salinity in NEMO. Ocean Modelling 67, 28–38.

Hieronymus, M., Nycander, J., Nilsson, J., Döös, K., Hallberg, R., 2019. Oceanic overturning and heat transport: The role of background diffusivity. J. Climate 32, 701–716.

Holland, W.R., 1978. The role of mesoscale eddies in the general circulation of the ocean–numerical experiments using a wind-driven quasi-geostrophic model. J. Phys. Oceanogr. 8, 363–392.

Holmes, R.M., de Lavergne, C., McDougall, T.J., 2018b. Ridges, seamounts, troughs, and bowls: Topographic control of the dianeutral circulation in the abyssal ocean. J. Phys. Oceanogr. 48, 861–882.

Holmes, R.M., Zika, J.D., England, M.H., 2018a. Diathermal heat transport in a global ocean model. J. Phys. Oceanogr. 49, 141–161.

Holmes, R.M., Zika, J.D., Ferrari, R., Thompson, A.F., Newsom, E.R., England, M.H., 2019. Atlantic ocean heat transport enabled by Indo-Pacific heat uptake and mixing. Geophysical Research Letters 46, 13939–13949.

Holzer, M., Primeau, F.W., 2006. The diffusive ocean conveyor. Geophysical Research Letters 33, L14618.

1095 Howard, E., Hogg, A.McC., Waterman, S., Marshall, D.P., 2014. The injection of zonal mo-
1096 mentum by buoyancy forcing in a Southern Ocean model. J. Phys. Oceanogr. 45, 259–271.
1097 Huang, R.X., 1999. Mixing and energetics of the oceanic thermohaline circulation. J. Phys.
1098 Oceanogr. 29, 727–746.
1099 Hughes, C.W., de Cuevas, B.A., 2001. Why western boundary currents in realistic oceans are
1100 inviscid: A link between form stress and bottom pressure torques. J. Phys. Oceanogr. 31,
1101 2871–2885.
1102 Hummels, R., Dengler, M., Bourlès, B., 2013. Seasonal and regional variability of upper ocean
1103 diapycnal heat flux in the Atlantic cold tongue. Progress in Oceanography 111, 52–74.
1104 Iselin, C.O., 1939. The influence of vertical and lateral turbulence on the characteristics of the
1105 waters at mid-depths. Eos, Transactions American Geophysical Union 20, 414–417.
1106 Iudicone, D., Madec, G., Blanke, B., Speich, S., 2008. The role of Southern Ocean surface
1107 forcings and mixing in the global conveyor. J. Phys. Oceanogr. 38, 1377–1400.
1108 Jackett, D.R., McDougall, T.J., 1997. A neutral density variable for the World's Oceans. J.
1109 Phys. Oceanogr. 27, 237–263.
1110 Jayne, S.R., 2009. The impact of abyssal mixing parameterizations in an ocean general circula-
1111 tion model. J. Phys. Oceanogr. 39, 1756–1775.
1112 Jing, Z., Wu, L., 2014. Intensified diapycnal mixing in the midlatitude western boundary cur-
1113 rents. Sci. Rep. 4.
1114 Jochum, M., Briegleb, B.P., Danabasoglu, G., Large, W.G., Norton, N.J., Jayne, S.R., Alford,
1115 M.H., Bryan, F.O., 2012. The impact of oceanic near-inertial waves on climate. J. Climate
1116 26, 2833–2844.
1117 Johnson, G.C., Bryden, H.L., 1989. On the size of the Antarctic Circumpolar Current. Deep
1118 Sea Research 36, 39–53.
1119 Jones, C.S., Abernathey, R.P., 2019. Isopycnal mixing controls deep ocean ventilation. Geo-

physical Research Letters 46, 13144–13151.

Klein, P., Treguier, A.-M., Hua, B.L., 1998. Three-dimensional stirring of thermohaline fronts. Journal of Marine Research 56, 589–612.

Klocker, A., Abernathey, R., 2014. Global patterns of mesoscale eddy properties and diffusivities. J. Phys. Oceanogr. 44, 1030–1046.

Klocker, A., McDougall, T.J., 2010. Influence of the nonlinear equation of state on global estimates of dianeutral advection and diffusion. J. Phys. Oceanogr. 40, 1690–1709.

Koch-Larrouy, A., Lengaigne, M., Terray, P., Madec, G., Masson, S., 2010. Tidal mixing in the Indonesian Seas and its effect on the tropical climate system. Climate Dynamics 34, 891–904.

Kunze, E., Firing, E., Hummon, J.M., Chereskin, T.K., Thurnherr, A.M., 2006. Global abyssal mixing inferred from lowered ADCP shear and CTD strain profiles. J. Phys. Oceanogr. 36, 1553-1576.

Lagerloef, G.S.E., Mitchum, G.T., Lukas, R.B., Niiler, P.P., 1999. Tropical Pacific near-surface currents estimated from altimeter, wind, and drifter data. J. Geophys. Res. 104, 23313–23326.

Large, W.G., McWilliams, J.C., Doney, S.C., 1994. Oceanic vertical mixing: A review and a model with a nonlocal boundary layer parameterization. Reviews of Geophysics 32, 363-403.

Le Corre, M., Gula, J., Tréguier, A.-M., 2020. Barotropic vorticity balance of the North Atlantic subpolar gyre in an eddy-resolving model. Ocean Science 16, 451–468.

Ledwell, J.R., St Laurent, L.C., Girton, J.B., Toole, J.M., 2011. Diapycnal mixing in the Antarctic Circumpolar Current. J. Phys. Oceanogr. 41, 241-246.

Ledwell, J.R., Montgomery, E.T., Polzin, K.L., St Laurent, L.C., Schmitt, R.W., Toole, J.M., 2000. Evidence for enhanced mixing over rough topography in the abyssal ocean. Nature 403, 179–182.

Ledwell, J.R., Watson, A.J., Law, C.S., 1998. Mixing of a tracer in the pycnocline. J. Geophys.

Res. 103, 21499–21529.

Ledwell, J.R., Watson, A.J., Law, C.S., 1993. Evidence for slow mixing across the pycnocline from an open-ocean tracer-release experiment. Nature 364, 701–703.

Locarnini, R.A., Mishonov, A.V., Baranova, O.K., Boyer, T.P., Zweng, M.M., Garcia, H.E., Reagan, J.R., Seidov, D., Weathers, K., Paver, C.R., Smolyar, I., 2018. World Ocean Atlas 2018, Volume 1: Temperature. A. Mishonov Technical Ed.; NOAA Atlas NESDIS 81, 52 pp.

Lozier, M.S., Li, F., Bacon, S., Bahr, F., Bower, A.S., Cunningham, S.A., Jong, M.F. de, Steur, L. de, deYoung, B., Fischer, J., Gary, S.F., Greenan, B.J.W., Holliday, N.P., Houk, A., Houpert, L., Inall, M.E., Johns, W.E., Johnson, H.L., Johnson, C., Karstensen, J., Koman, G., Bras, I.A.L., Lin, X., Mackay, N., Marshall, D.P., Mercier, H., Oltmanns, M., Pickart, R.S., Ramsey, A.L., Rayner, D., Straneo, F., Thierry, V., Torres, D.J., Williams, R.G., Wilson, C., Yang, J., Yashayaev, I., Zhao, J., 2019. A sea change in our view of overturning in the subpolar North Atlantic. Science 363, 516–521.

Lu, P., McCreary, J.P., Klinger, B.A., 1998. Meridional circulation cells and the source waters of the Pacific equatorial undercurrent. J. Phys. Oceanogr. 28, 62-84.

Lucazeau, F., 2019. Analysis and mapping of an updated terrestrial heat flow data set. Geochemistry, Geophysics, Geosystems 20, 4001–4024.

Lumpkin, R., Speer, K., 2007. Global ocean meridional overturning. J. Phys. Oceanogr. 37, 2550–2562.

Lumpkin, R., Speer, K., 2003. Large-scale vertical and horizontal circulation in the North Atlantic ocean. J. Phys. Oceanogr. 33, 1902–1920.

Luyten, J.R., Pedlosky, J., Stommel, H., 1983. The ventilated thermocline. J. Phys. Oceanogr. 13, 292–309.

MacKinnon, J.A., Johnston, T.M.S., Pinkel, R., 2008. Strong transport and mixing of deep water through the Southwest Indian Ridge. Nature Geoscience 1, 755–758.

Mantyla, A.W., Reid, J.L., 1983. Abyssal characteristics of the World Ocean waters. Deep Sea Research 30, 805–833.

Marshall, D., 1997. Subduction of water masses in an eddying ocean. Journal of Marine Research 55, 201–222.

Marshall, J.C., Nurser, A.J.G., 1991. A continuously stratified thermocline model incorporating a mixed layer of variable thickness and density. J. Phys. Oceanogr. 21, 1780–1792.

Marshall, J., Jones, H., Karsten, R., Wardle, R., 2002. Can eddies set ocean stratification? J. Phys. Oceanogr. 32, 26–38.

Marshall, J., Radko, T., 2003. Residual-mean solutions for the Antarctic Circumpolar Current and its associated overturning circulation. J. Phys. Oceanogr. 33, 2341–2354.

Marshall, J., Speer, K., 2012. Closure of the meridional overturning circulation through Southern Ocean upwelling. Nature Geoscience 5, 171–180.

Mashayek, A., Ferrari, R., Merrifield, S., Ledwell, J.R., Laurent, L.S., Naveira Garabato, A.C., 2017. Topographic enhancement of vertical turbulent mixing in the Southern Ocean. Nature Communications 8, 14197.

Mazloff, M.R., Ferrari, R., Schneider, T., 2013. The force balance of the Southern Ocean meridional overturning circulation. J. Phys. Oceanogr. 43, 1193-1208.

McCartney, M.S., 1977. Subantarctic Mode Water. In. A Voyage of Discovery, Deep Sea Research 24, 103–119.

McCreary, J.P., Lu, P., 1994. Interaction between the subtropical and equatorial ocean circulations: The subtropical cell. J. Phys. Oceanogr. 24, 466–497.

McDougall, T.J., 2003. Potential enthalpy: A conservative oceanic variable for evaluating heat content and heat fluxes. J. Phys. Oceanogr. 33, 945–963.

McDougall, T.J., 1984. The relative roles of diapycnal and isopycnal mixing on subsurface water mass conversion. J. Phys. Oceanogr. 14, 1577–1589.

McDougall, T.J., 1989. Dianeutral advection. *Parameterization of small-scale processes: Proc. 'Aha Huliko'a Hawaiian Winter Workshop*, Honolulu, HI, University of Hawaii at Manoa, 289-315.

McDougall, T.J., Ferrari, R., 2017. Abyssal upwelling and downwelling driven by near-boundary mixing. J. Phys. Oceanogr. 47, 261–283.

McDougall, T.J., Groeskamp, S., Griffies, S.M., 2014. On geometrical aspects of interior ocean mixing. J. Phys. Oceanogr. 44, 2164–2175.

McDougall, T.J., Jackett, D.R., Millero, F.J., Pawlowicz, R., Barker, P.M., 2012. A global algorithm for estimating Absolute Salinity. Ocean Science 8, 1123–1134.

McDougall, T.J., McIntosh, P.C., 2001. The temporal-residual-mean velocity. Part II: Isopycnal interpretation and the tracer and momentum equations. J. Phys. Oceanogr. 31, 1222–1246.

McPhaden, M.J., Zhang, D., 2002. Slowdown of the meridional overturning circulation in the upper Pacific Ocean. Nature 415, 603–608.

McWilliams, J.C., Chow, J.H.S., 1981. Equilibrium geostrophic turbulence I: A reference solution in a β-plane channel. J. Phys. Oceanogr. 11, 921–949.

Melet, A., Hallberg, R., Legg, S., Nikurashin, M., 2014. Sensitivity of the ocean state to lee wave–driven mixing. J. Phys. Oceanogr. 44, 900–921.

Melet, A., Legg, S., Hallberg, R., 2016. Climatic impacts of parameterized local and remote tidal mixing. J. Climate 29, 3473–3500.

Mercier, H., Speer, K.G., 1998. Transport of bottom water in the Romanche fracture zone and the Chain fracture zone. J. Phys. Oceanogr. 28, 779–790.

Meredith, M.P., Woodworth, P.L., Chereskin, T.K., Marshall, D.P., Allison, L.C., Bigg, G.R., Donohue, K., Heywood, K.J., Hughes, C.W., Hibbert, A., Hogg, A.M., Johnson, H.L., Jullion, L., King, B.A., Leach, H., Lenn, Y.-D., Maqueda, M.A.M., Munday, D.R., Naveira Garabato, A.C., Provost, C., Sallée, J.-B., Sprintall, J., 2011. Sustained monitoring of the

1220 Southern Ocean at Drake Passage: Past achievements and future priorities. Reviews of Geo-
1221 physics 49.
1222 Moum, J.N., Lien, R.-C., Perlin, A., Nash, J.D., Gregg, M.C., Wiles, P.J., 2009. Sea surface
1223 cooling at the Equator by subsurface mixing in tropical instability waves. Nature Geoscience
1224 2, 761–765.
1225 Moum, J.N., Perlin, A., Nash, J.D., McPhaden, M.J., 2013. Seasonal sea surface cooling in the
1226 equatorial Pacific cold tongue controlled by ocean mixing. Nature 500, 64–67.
1227 Munday, D.R., Allison, L.C., Johnson, H.L., Marshall, D.P., 2011. Remote forcing of the
1228 Antarctic Circumpolar Current by diapycnal mixing. Geophysical Research Letters 38, L08609.
1229 Munk, W., 1997. Once again: once again—tidal friction. Progress in Oceanography 40, 7–35.
1230 Munk, W., Wunsch, C., 1998. Abyssal recipes II: Energetics of tidal and wind mixing. Deep-
1231 Sea Research 45, 1977–2010.
1232 Munk, W.H., 1966. Abyssal recipes. Deep Sea Research 13, 707–730.
1233 Munk, W.H., 1950. On the wind-driven ocean circulation. J. Meteor. 7, 80–93.
1234 Munk, W.H., Palmén, E., 1951. Note on the dynamics of the Antarctic Circumpolar Current.
1235 Tellus 3, 53–55.
1236 Naveira Garabato, A.C., Frajka-Williams, E., Spingys, C.P., Legg, S., Polzin, K.L., Forryan,
1237 A., Abrahamsen, P., Buckingham, C., Griffies, S.M., McPhail, S., Nicholls, K., Thomas,
1238 L.N., Meredith, M., 2019. Rapid mixing and exchange of deep-ocean waters in an abyssal
1239 boundary current. Proceedings of the National Academy of Sciences 116, 13233–13238.
1240 Naveira Garabato, A.C., MacGilchrist, G.A., Brown, P.J., Evans, D.G., Meijers, A.J.S., Zika,
1241 J.D., 2017. High-latitude ocean ventilation and its role in Earth's climate transitions. Phil.
1242 Trans. R. Soc. A 375, 20160324.
1243 Naveira Garabato, A.C., Polzin, K.L., Ferrari, R., Zika, J.D., Forryan, A., 2016. A microscale
1244 view of mixing and overturning across the Antarctic Circumpolar Current. J. Phys. Oceanogr.

46, 233–254.

Naveira Garabato, A.C., Stevens, D.P., Watson, A.J., Roether, W., 2007. Short-circuiting of the overturning circulation in the Antarctic Circumpolar Current. Nature 447, 194–197.

Naveira Garabato, A.C., Williams, A.P., Bacon, S., 2014. The three-dimensional overturning circulation of the Southern Ocean during the WOCE era. Progress in Oceanography 120, 41–78.

Nikurashin, M., Vallis, G., 2012. A theory of the interhemispheric meridional overturning circulation and associated stratification. J. Phys. Oceanogr. 42, 1652–1667.

Nurser, A.J.G., Marsh, R., Williams, R.G., 1999. Diagnosing water mass formation from air-sea fluxes and surface mixing. J. Phys. Oceanogr. 29, 1468–1487.

Nycander, J., Hieronymus, M., Roquet, F., 2015. The nonlinear equation of state of sea water and the global water mass distribution. Geophysical Research Letters 42, 2015GL065525.

Nycander, J., Nilsson, J., Döös, K., Broström, G., 2007. Thermodynamic analysis of ocean circulation. J. Phys. Oceanogr. 37, 2038–2052.

Oakey, N.S., 1982. Determination of the rate of dissipation of turbulent energy from simultaneous temperature and velocity shear microstructure Mmeasurements. J. Phys. Oceanogr. 12, 256–271.

Olbers, D., 1998. Comments on "On the obscurantist physics of 'Form Drag' in theorizing about the Circumpolar Current." J. Phys. Oceanogr. 28, 1647–1654.

Orsi, A.H., Johnson, G.C., Bullister, J.L., 1999. Circulation, mixing, and production of Antarctic Bottom Water. Progress in Oceanography 43, 55–109.

Osborn, T.R., 1978. Measurements of energy dissipation adjacent to an island. J. Geophys. Res. 83, 2939.

Osborn, T.R., Cox, C.S., 1972. Oceanic fine structure. Geophysical Fluid Dynamics 3, 321–345.

Pacanowski, R.C., 1987. Effect of equatorial currents on surface stress. J. Phys. Oceanogr. 17,

833–838.

Pedlosky, J., 1996. Ocean circulation theory. Springer, Berlin, 453 pp.

Pedlosky, J., 1992. The baroclinic structure of the abyssal circulation. J. Phys. Oceanogr. 22, 652–659.

Pellichero, V., Sallée, J.-B., Schmidtko, S., Roquet, F., Charrassin, J.-B., 2017. The ocean mixed layer under Southern Ocean sea-ice: Seasonal cycle and forcing. J. Geophys. Res. 122, 1608–1633.

PeñaMolino, B., Rintoul, S.R., Mazloff, M.R., 2014. Barotropic and baroclinic contributions to along-stream and across-stream transport in the Antarctic Circumpolar Current. J. Geophys. Res. 119, 8011–8028.

Pickart, R.S., Spall, M.A., 2007. Impact of Labrador Sea convection on the North Atlantic meridional overturning circulation. J. Phys. Oceanogr. 37, 2207–2227.

Plant, W.J., 1982. A relationship between wind stress and wave slope. J. Geophys. Res. 87, 1961–1967.

Pollard, R.T., Rhines, P.B., Thompson, R.O., 1973. The deepening of the wind-mixed layer. Geophys. Astrophys. Fluid Dyn. 4, 381–404.

Polzin, K.L., Speer, K.G., Toole, J.M., Schmitt, R.W., 1996. Intense mixing of Antarctic Bottom Water in the equatorial Atlantic Ocean. Nature 380, 54–57.

Polzin, K.L., Toole, J.M., Ledwell, J.R., Schmitt, R.W., 1997. Spatial variability of turbulent mixing in the abyssal ocean. Science 276, 93–96.

Price, J.F., Weller, R.A., Pinkel, R., 1986. Diurnal cycling: Observations and models of the upper ocean response to diurnal heating, cooling, and wind mixing. J. Geophys. Res. 91, 8411-8427.

Price, J.F., 2001. Chapter 5.3 - Subduction, in: Siedler, G., Church, J., Gould, J. (Eds.), International Geophysics, Ocean Circulation and Climate. Academic Press, pp. 357–371.

Pujol, M.-I., Faugère, Y., Taburet, G., Dupuy, S., Pelloquin, C., Ablain, M., Picot, N., 2016. DUACS DT2014: the new multi-mission altimeter data set reprocessed over 20 years. Ocean Science 12, 1067–1090.

Qu, T., Gao, S., Fine, R.A., 2013. Subduction of South Pacific tropical water and its equatorward pathways as shown by a simulated passive tracer. J. Phys. Oceanogr. 43, 1551-1565.

Ragen, S., Pradal, M.-A., Gnanadesikan, A., 2020. The impact of parameterized lateral mixing on the Antarctic Circumpolar Current in a coupled climate model. J. Phys. Oceanogr. 50, 965–982.

Reid, J.L., 2003. On the total geostrophic circulation of the Indian ocean: flow patterns, tracers, and transports. Progress in Oceanography 56, 137–186.

Reid, J.L., 1997. On the total geostrophic circulation of the Pacific ocean: flow patterns, tracers, and transports. Progress in Oceanography 39, 263–352.

Rhines, P.B., 1993. Oceanic General Circulation: Wave and Advection Dynamics, in: Willebrand, J., Anderson, D.L.T. (Eds.), Modelling Oceanic Climate Interactions, NATO ASI Series. Springer, Berlin, Heidelberg, pp. 67–149.

Rhines, P.B., Holland, W.R., 1979. A theoretical discussion of eddy-driven mean flows. Dynamics of Atmospheres and Oceans 3, 289–325.

Rhines, P.B., Young, W.R., 1982. Homogenization of potential vorticity in planetary gyres. Journal of Fluid Mechanics 122, 347–367.

Rintoul, S.R., Naveira Garabato, A.C., 2013. Chapter 18 - Dynamics of the Southern Ocean Circulation, in: Siedler, G., Griffies, S.M., Gould, J., Church, J.A. (Eds.), International Geophysics, Ocean Circulation and Climate. Academic Press, pp. 471–492.

Robbins, P.E., Price, J.F., Owens, W.B., Jenkins, W.J., 2000. The importance of lateral diffusion for the ventilation of the lower thermocline in the subtropical North Atlantic. J. Phys. Oceanogr. 30, 67–89.

Roemmich, D., 1983. The balance of geostrophic and Ekman transports in the tropical Atlantic Ocean. J. Phys. Oceanogr. 13, 1534–1539.

Roquet, F., Wunsch, C., Madec, G., 2011. On the patterns of wind-power input to the ocean circulation. J. Phys. Oceanogr. 41, 2328–2342.

Rudnick, D.L., Boyd, T.J., Brainard, R.E., Carter, G.S., Egbert, G.D., Gregg, M.C., Holloway, P.E., Klymak, J.M., Kunze, E., Lee, C.M., Levine, M.D., Luther, D.S., Martin, J.P., Merrifield, M.A., Moum, J.N., Nash, J.D., Pinkel, R., Rainville, L., Sanford, T.B., 2003. From tides to mixing along the Hawaiian ridge. Science 301, 355-357.

Samelson, R.M., Vallis, G.K., 1997. Large-scale circulation with small diapycnal diffusion: The two-thermocline limit. Journal of Marine Research 55, 223–275.

Sarmiento, J.L., Simeon, J., Gnanadesikan, A., Gruber, N., Key, R.M., Schlitzer, R., 2007. Deep ocean biogeochemistry of silicic acid and nitrate. Global Biogeochemical Cycles 21, GB1S90.

Sasaki, H., Kida, S., Furue, R., Nonaka, M., Masumoto, Y., 2018. An increase of the Indonesian Throughflow by internal tidal mixing in a high-resolution quasi-global ocean simulation. Geophysical Research Letters 45, 8416–8424.

Schmitz, W.J., 1995. On the interbasin-scale thermohaline circulation. Rev. Geophys. 33, 151–173.

Schmitz, W.J., Richardson, P.L., 1991. On the sources of the Florida Current. Deep-Sea Res. 38, S379–S409.

Sheen, K.L., Brearley, J.A., Naveira Garabato, A.C., Smeed, D.A., Waterman, S., Ledwell, J.R., Meredith, M.P., St. Laurent, L., Thurnherr, A.M., Toole, J.M., Watson, A.J., 2013. Rates and mechanisms of turbulent dissipation and mixing in the Southern Ocean: Results from the Diapycnal and Isopycnal Mixing Experiment in the Southern Ocean (DIMES). J. Geophys. Res. 118, 2774–2792.

Sloyan, B.M., Johnson, G.C., Kessler, W.S., 2003. The Pacific cold tongue: A pathway for interhemispheric exchange. J. Phys. Oceanogr. 33, 1027–1043.

Sloyan, B.M., Rintoul, S.R., 2001. The Southern Ocean limb of the global deep overturning circulation. J. Phys. Oceanogr. 31, 143–173.

Sloyan, B.M., Talley, L.D., Chereskin, T.K., Fine, R., Holte, J., 2010. Antarctic Intermediate Water and Subantarctic Mode Water formation in the southeast Pacific: The role of turbulent mixing. J. Phys. Oceanogr. 40, 1558–1574.

Smith, K.S., Ferrari, R., 2009. The production and dissipation of compensated thermohaline variance by mesoscale stirring. J. Phys. Oceanogr. 39, 2477–2501.

Smith, R.D., McWilliams, J.C., 2003. Anisotropic horizontal viscosity for ocean models. Ocean Modelling 5, 129–156.

Smyth, W.D., Moum, J.N., 2013. Marginal instability and deep cycle turbulence in the eastern equatorial Pacific Ocean. Geophysical Research Letters 40, 6181–6185.

St. Laurent, L., Naveira Garabato, A.C., Ledwell, J.R., Thurnherr, A.M., Toole, J.M., Watson, A.J., 2012. Turbulence and diapycnal mixing in Drake Passage. J. Phys. Oceanogr. 42, 2143–2152.

St. Laurent, L.C., Toole, J.M., Schmitt, R.W., 2001. Buoyancy forcing by turbulence above rough topography in the abyssal Brazil Basin. J. Phys. Oceanogr. 31, 3476–3495.

Stewart, A.L., Hogg, A.McC., 2017. Reshaping the Antarctic Circumpolar Current via Antarctic Bottom Water export. J. Phys. Oceanogr. 47, 2577–2601.

Stommel, H., 1979. Determination of water mass properties of water pumped down from the Ekman layer to the geostrophic flow below. Proceedings of National Academy of Sciences 76, 3051–3055.

Stommel, H., 1958. The abyssal circulation. Deep Sea Research 5, 80–82.

Stommel, H., Arons, A.B., 1959a. On the abyssal circulation of the world ocean—II. An ideal-

ized model of the circulation pattern and amplitude in oceanic basins. Deep Sea Research 6, 217–233.

Stommel, H., Arons, A.B., 1959b. On the abyssal circulation of the world ocean—I. Stationary planetary flow patterns on a sphere. Deep Sea Research 6, 140–154.

Su, Z., Stewart, A.L., Thompson, A.F., 2014. An idealized model of Weddell Gyre export variability. J. Phys. Oceanogr. 44, 1671-1688.

Sun, S., Eisenman, I., Zanna, L., Stewart, A.L., 2020. Surface constraints on the depth of the Atlantic meridional overturning circulation: Southern Ocean versus North Atlantic. J. Climate 33, 3125–3149.

Sweeney, C., Gnanadesikan, A., Griffies, S.M., Harrison, M.J., Rosati, A.J., Samuels, B.L., 2005. Impacts of shortwave penetration depth on large-scale ocean circulation and heat transport. J. Phys. Oceanogr. 35, 1103–1119.

Taburet, G., Sanchez-Roman, A., Ballarotta, M., Pujol, M.-I., Legeais, J.-F., Fournier, F., Faugere, Y., Dibarboure, G., 2019. DUACS DT2018: 25 years of reprocessed sea level altimetry products. Ocean Science 15, 1207–1224.

Talley, L., 2013. Closure of the global overturning circulation through the Indian, Pacific, and Southern Oceans: Schematics and transports. Oceanography 26, 80–97.

Tamsitt, V., Abernathey, R.P., Mazloff, M.R., Wang, J., Talley, L.D., 2018. Transformation of deep water masses along Lagrangian upwelling pathways in the Southern Ocean. J. Geophys. Res. 123, 1994–2017.

Tamsitt, V., Drake, H.F., Morrison, A.K., Talley, L.D., Dufour, C.O., Gray, A.R., Griffies, S.M., Mazloff, M.R., Sarmiento, J.L., Wang, J., Weijer, W., 2017. Spiraling pathways of global deep waters to the surface of the Southern Ocean. Nature Communications 8, 172.

Thompson, A.F., Stewart, A.L., Spence, P., Heywood, K.J., 2018. The Antarctic slope current in a changing climate. Reviews of Geophysics 56, 741–770.

Toggweiler, J.R., Druffel, E.R.M., Key, R.M., Galbraith, E.D., 2019a. Upwelling in the ocean basins north of the ACC: 1. On the upwelling exposed by the surface distribution of Δ^{14}C. J. Geophys. Res. 124, 2591–2608.

Toggweiler, J.R., Druffel, E.R.M., Key, R.M., Galbraith, E.D., 2019b. Upwelling in the ocean basins north of the ACC: 2. How cool subantarctic water reaches the surface in the tropics. J. Geophys. Res. 124, 2609–2625.

Toggweiler, J.R., Samuels, B., 1998. On the ocean's large-scale circulation near the limit of no vertical mixing. J. Phys. Oceanogr. 28, 1832–1852.

Toggweiler, J.R., Samuels, B., 1995. Effect of Drake Passage on the global thermohaline circulation. Deep Sea Research 42, 477–500.

Toggweiler, J.R., Samuels, B., 1993. New Radiocarbon Constraints on the Upwelling of Abyssal Water to the Ocean's Surface, in: Heimann, M. (Ed.), The Global Carbon Cycle, NATO ASI Series. Springer Berlin Heidelberg, pp. 333–366.

Toole, J.M., Schmitt, R.W., Polzin, K.L., 1994. Estimates of diapycnal mixing in the abyssal ocean. Science 264, 1120–1123.

Treguier, A.M., Held, I.M., Larichev, V.D., 1997. Parameterization of quasigeostrophic eddies in primitive equation ocean models. J. Phys. Oceanogr. 27, 567–580.

Urakawa, L.S., Hasumi, H., 2012. Eddy-resolving model estimate of the cabbeling effect on the water mass transformation in the Southern Ocean. J. Phys. Oceanogr. 42, 1288–1302.

van Haren, H., Gostiaux, L., 2012. Detailed internal wave mixing above a deep-ocean slope. Journal of Marine Research 70, 173-197.

Vic, C., Naveira Garabato, A.C., Green, J.A.M., Waterhouse, A.F., Zhao, Z., Melet, A., Lavergne, C. de, Buijsman, M.C., Stephenson, G.R., 2019. Deep-ocean mixing driven by small-scale internal tides. Nature Communications 10, 2099.

Voet, G., Girton, J.B., Alford, M.H., Carter, G.S., Klymak, J.M., Mickett, J.B., 2014. Pathways,

volume transport, and mixing of abyssal water in the Samoan Passage. J. Phys. Oceanogr. 45, 562–588.

Walin, G., 1982. On the relation between sea-surface heat flow and thermal circulation in the ocean. Tellus 34, 187–195.

Walin, G., 1977. A theoretical framework for the description of estuaries. Tellus 29, 128–136.

Wang, Z., Meredith, M.P., 2008. Density-driven southern hemisphere subpolar gyres in coupled climate models. Geophysical Research Letters 35, L14608.

Waterhouse, A.F., MacKinnon, J.A., Nash, J.D., Alford, M.H., Kunze, E., Simmons, H.L., Polzin, K.L., St. Laurent, L.C., Sun, O.M., Pinkel, R., Talley, L.D., Whalen, C.B., Huussen, T.N., Carter, G.S., Fer, I., Waterman, S., Naveira Garabato, A.C., Sanford, T.B., Lee, C.M., 2014. Global patterns of diapycnal mixing from measurements of the turbulent dissipation rate. J. Phys. Oceanogr. 44, 1854–1872.

Watson, A.J., Ledwell, J.R., Messias, M.-J., King, B.A., Mackay, N., Meredith, M.P., Mills, B., Naveira Garabato, A.C., 2013. Rapid cross-density ocean mixing at mid-depths in the Drake Passage measured by tracer release. Nature 501, 408–411.

Whalen, C.B., MacKinnon, J.A., Talley, L.D., 2018. Large-scale impacts of the mesoscale environment on mixing from wind-driven internal waves. Nature Geoscience 11, 842.

Wolfe, C.L., Cessi, P., 2011. The adiabatic pole-to-pole overturning circulation. J. Phys. Oceanogr. 41, 1795–1810.

Wunsch, C., 1997. The vertical partition of oceanic horizontal kinetic energy. J. Phys. Oceanogr. 27, 1770–1794.

Wunsch, C., 1970. On oceanic boundary mixing. Deep Sea Research 17, 293–301.

Wunsch, C., Ferrari, R., 2004. Verrtical mixing, energy, and the general circulation of the oceans. Annual Review of Fluid Mechanics 36, 281–314.

Yang, X., Tziperman, E., Speer, K., 2020. Dynamics of deep ocean eastern boundary currents.

Geophysical Research Letters 47, e2019GL085396.

Zhai, X., Greatbatch, R.J., Eden, C., Hibiya, T., 2009. On the loss of wind-induced near-inertial energy to turbulent mixing in the upper ocean. J. Phys. Oceanogr. 39, 3040–3045.

Zhai, X., Johnson, H.L., Marshall, D.P., 2010. Significant sink of ocean-eddy energy near western boundaries. Nature Geoscience 3, 608–612.

Zhang, R., Delworth, T.L., Rosati, A., Anderson, W.G., Dixon, K.W., Lee, H.-C., Zeng, F., 2011. Sensitivity of the North Atlantic ocean circulation to an abrupt change in the Nordic Sea overflow in a high resolution global coupled climate model. J. Geophys. Res. 116, C12024.

Zhu, Y., Zhang, R.-H., 2019. A modified vertical mixing parameterization for its improved ocean and coupled simulations in the tropical Pacific. J. Phys. Oceanogr. 49, 21–37.

Zika, J.D., Le Sommer, J., Dufour, C.O., Molines, J.-M., Barnier, B., Brasseur, P., Dussin, R., Penduff, T., Iudicone, D., Lenton, A., Madec, G., Mathiot, P., Orr, J., Shuckburgh, E., Vivier, F., 2012. Vertical eddy fluxes in the Southern Ocean. J. Phys. Oceanogr. 43, 941–955.

Zika, J.D., Skliris, N., Nurser, A.J.G., Josey, S.A., Mudryk, L., Laliberté, F., Marsh, R., 2015. Maintenance and broadening of the ocean's salinity distribution by the water cycle. J. Climate 28, 9550–9560.

Zika, J.D., Sloyan, B.M., McDougall, T.J., 2009. Diagnosing the Southern Ocean overturning from tracer fields. J. Phys. Oceanogr. 39, 2926–2940.

Zweng, M. M., Reagan, J.R., Seidov, D., Boyer, T.P., Locarnini, R.A., Garcia, H.E., Mishonov, A.V., Baranova, O.K., Weathers, K., Paver, C.R., Smolyar, I., 2018. World Ocean Atlas 2018, Volume 2: Salinity. A. Mishonov Technical Ed.; NOAA Atlas NESDIS 82, 50 pp.

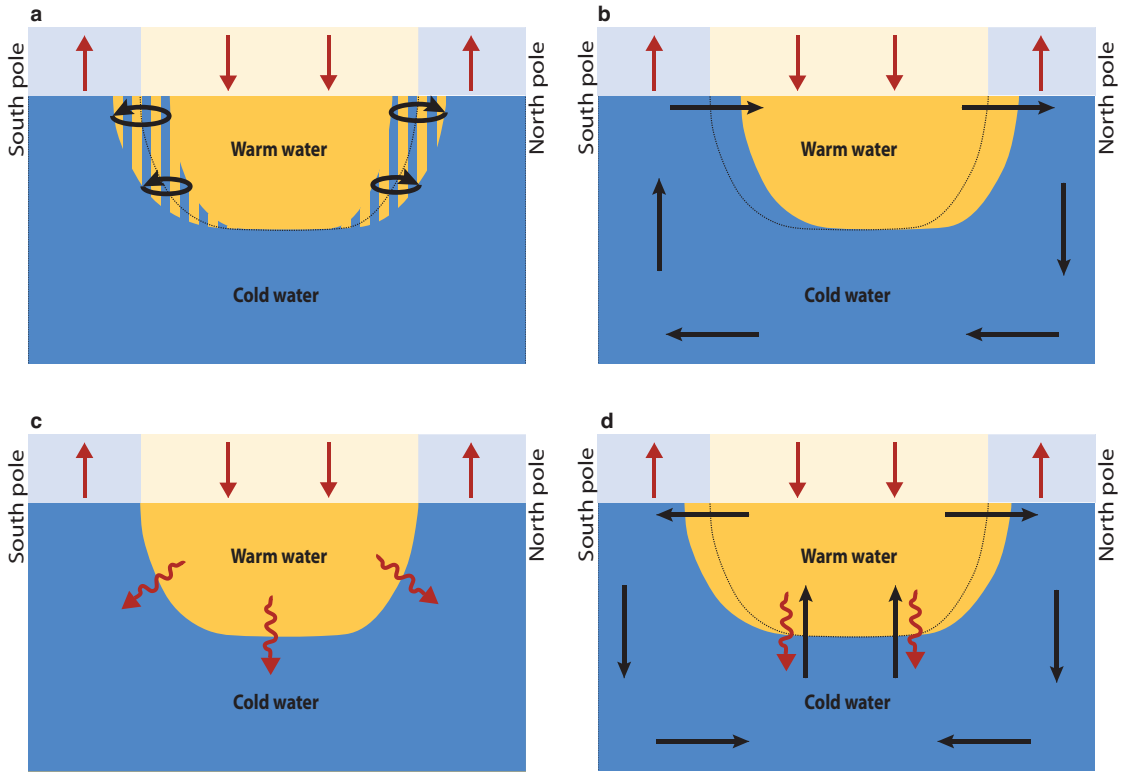

Figure 1: Idealised two-layer ocean composed of a warm bowl overlying a cold pool. Heating and cooling at the surface occurs within fixed latitudinal bands, represented by light blue (cooling) and light yellow (heating) colors. Salinity and freshwater fluxes are ignored. Straight and wiggly red arrows represent surface and interior heat fluxes, respectively. Black arrows represent mass transports. Each panel corresponds to a distinct scenario of poleward oceanic heat transport. Shown variations in the position and shape of the warm bowl are illustrative and partly arbitrary. **a**, Horizontal circulation moves warm water into the cooling latitudes and cold water into the warming latitudes. **b**, An inter-hemispheric overturning circulation shifts the warm bowl northward, reducing net heat gain (loss) of warm (cold) waters. **c**, Mixing transfers heat from the warm bowl to the cold pool. Note that we implicitly assume that mixing within each layer maintains temperature homogeneity, and thus connects surface and interior heat fluxes. **d**, Mixing converts cold waters into warm waters, allowing hemispheric overturning circulations to develop and transport heat poleward. Part of the diffusive heat gain of the lower layer may also offset surface cooling via intra-layer heat transports, as in **c**.

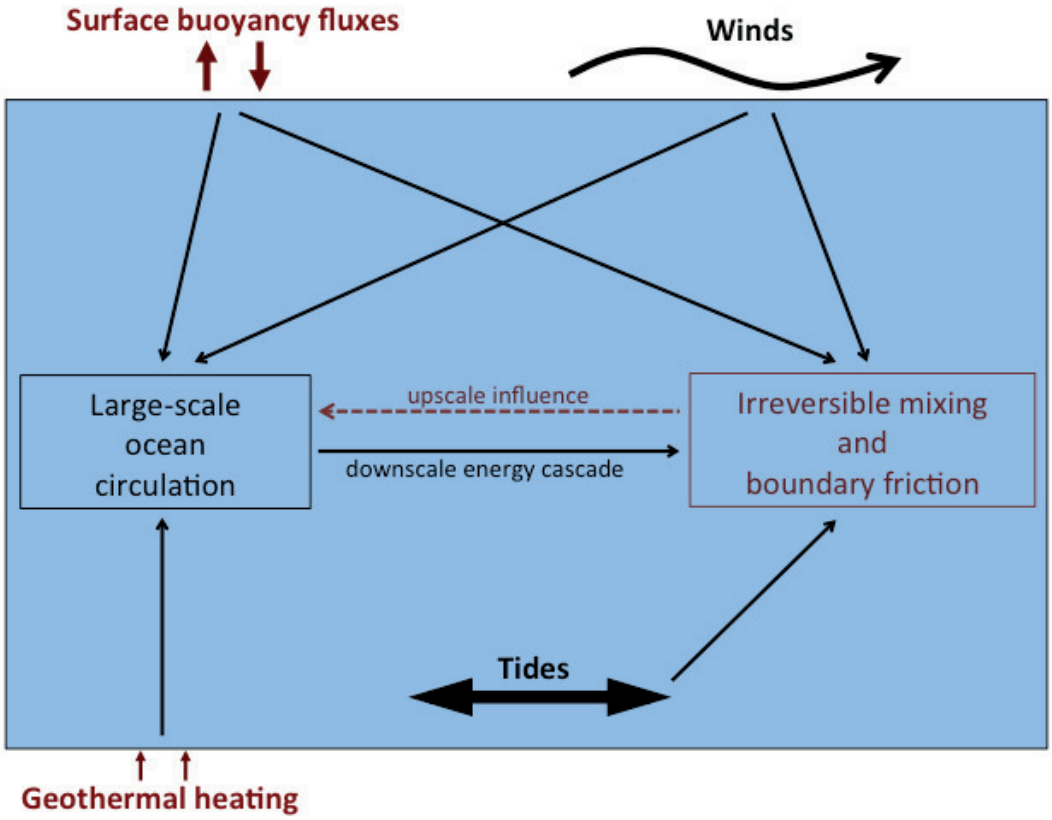

Figure 2: Simplified schematic of energy flows in the ocean, from forcing to dissipation. Forcing boils down to surface buoyancy fluxes, surface winds, tides (caused by gravitational interaction with the Moon and Sun), and geothermal heating along the seafloor. The large-scale ocean circulation is forced directly by large-scale wind and buoyancy forcing, and indirectly by irreversible mixing. Energy of the large-scale circulation is ultimately dissipated by boundary friction (drag) and irreversible mixing. Irreversible mixing includes momentum, temperature and salinity mixing at molecular scale. Mixing is energized directly by tides, winds, surface buoyancy fluxes and indirectly by the energy cascade from large-scale circulation to turbulence. Note that energy fuelling irreversible mixing and boundary friction is either lost as heat (momentum mixing and drag) or does work against gravity (mixing-driven buoyancy fluxes). The direct forcing of global ocean circulation by tides is thought to be secondary (Bessières et al. 2008) and is therefore not highlighted here, despite known contributions to regional circulation features (e.g., Thompson et al. 2018, Chapter 2).

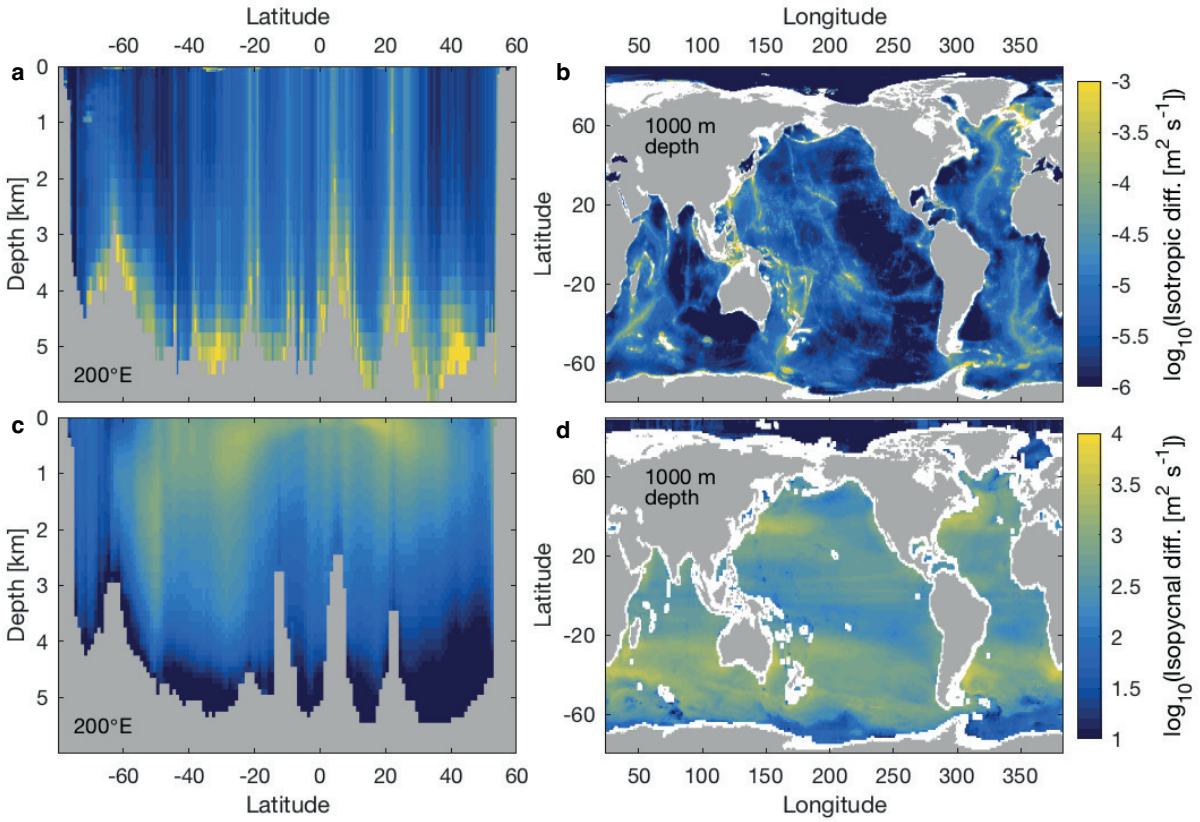

Figure 3: Estimated isotropic (**a,b**) and isopycnal (**c,d**) diffusivities, at 200°E/160°W (**a,c**) and at 1000 m depth (**b,d**). Both diffusivities are shown on a $\log_{10}$ scale that spans three orders of magnitude (see colorscales on the right). Isotropic diffusivity here only includes the contribution of internal waves energized by tides (de Lavergne et al. 2020). Isopycnal diffusivity quantifies rates of mesoscale stirring (Groeskamp et al. 2020).

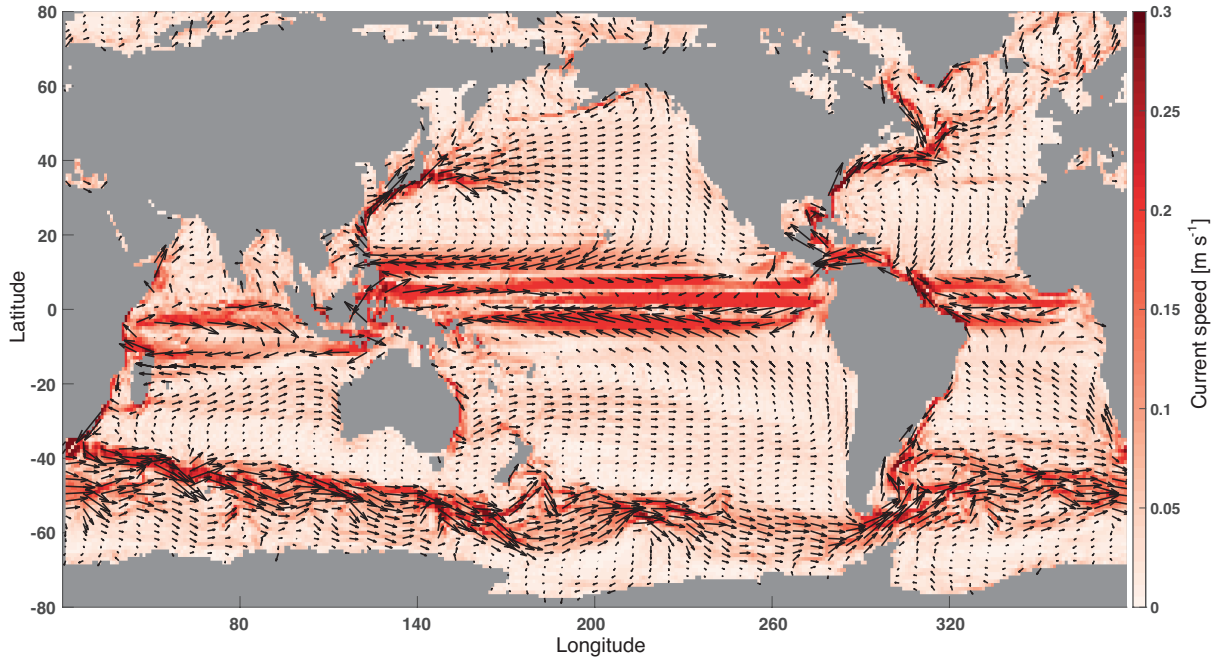

Figure 4: Annual mean surface geostrophic currents calculated using satellite observations. Surface geostrophic velocity obtained from the CMEMS (Copernicus Marine Environment Monitoring Service) operational delayed-time sea surface geostrophic velocity anomalies derived from satellite altimetry (Pujol et al. 2016, Taburet et al. 2019), using a β-plane approximation of the geostrophic equations in the equatorial band (Lagerhoef et al. 1999). Daily, quarter degree resolution data since 1993 is averaged and smoothed into a mean for illustrative purposes. Color is indicative of the speed, with darker colors being faster currents.

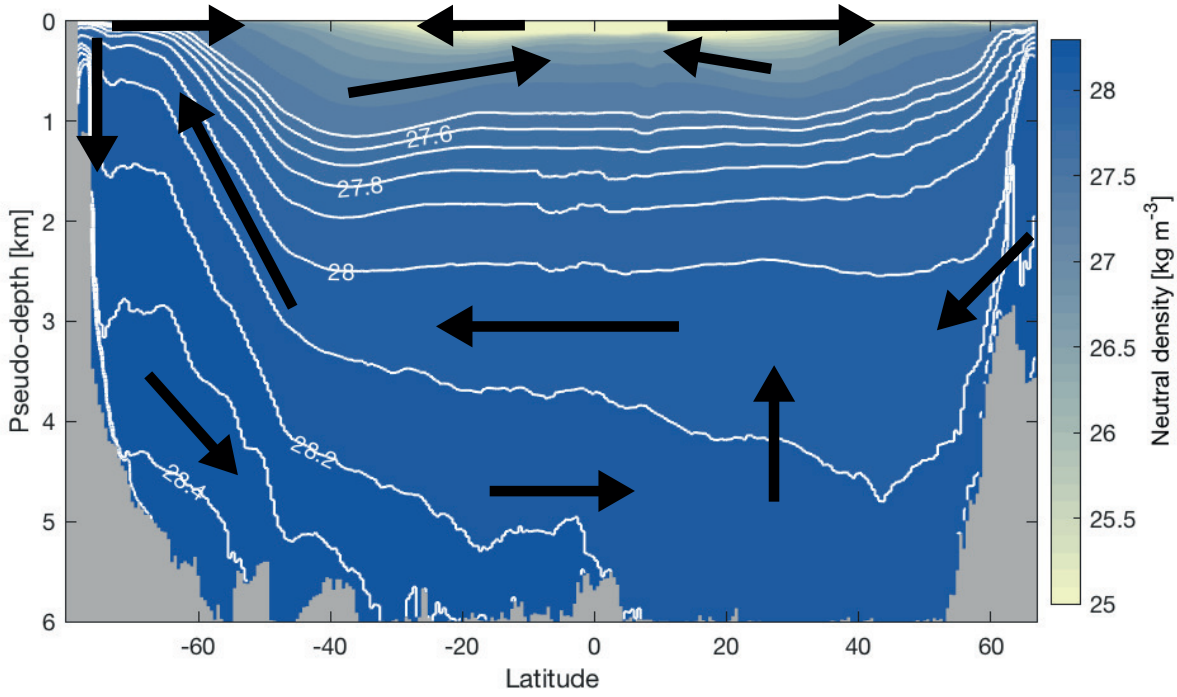

Figure 5: Global neutral density stratification and schematic meridional overturning circulation. The shading shows neutral density (Jackett and McDougall 1997) mapped by Gouretski and Koltermann (2004) as a function of latitude and pseudo-depth. The pseudo-depth of density surfaces is found by filling each latitude band from the bottom up with ocean grid cells ordered from dense to light. The neutral density range 27.5-28.5 kg m^{-3} is contoured in white with a 0.1 kg m^{-3} interval. Black arrows give a simplified view of overturning flows.

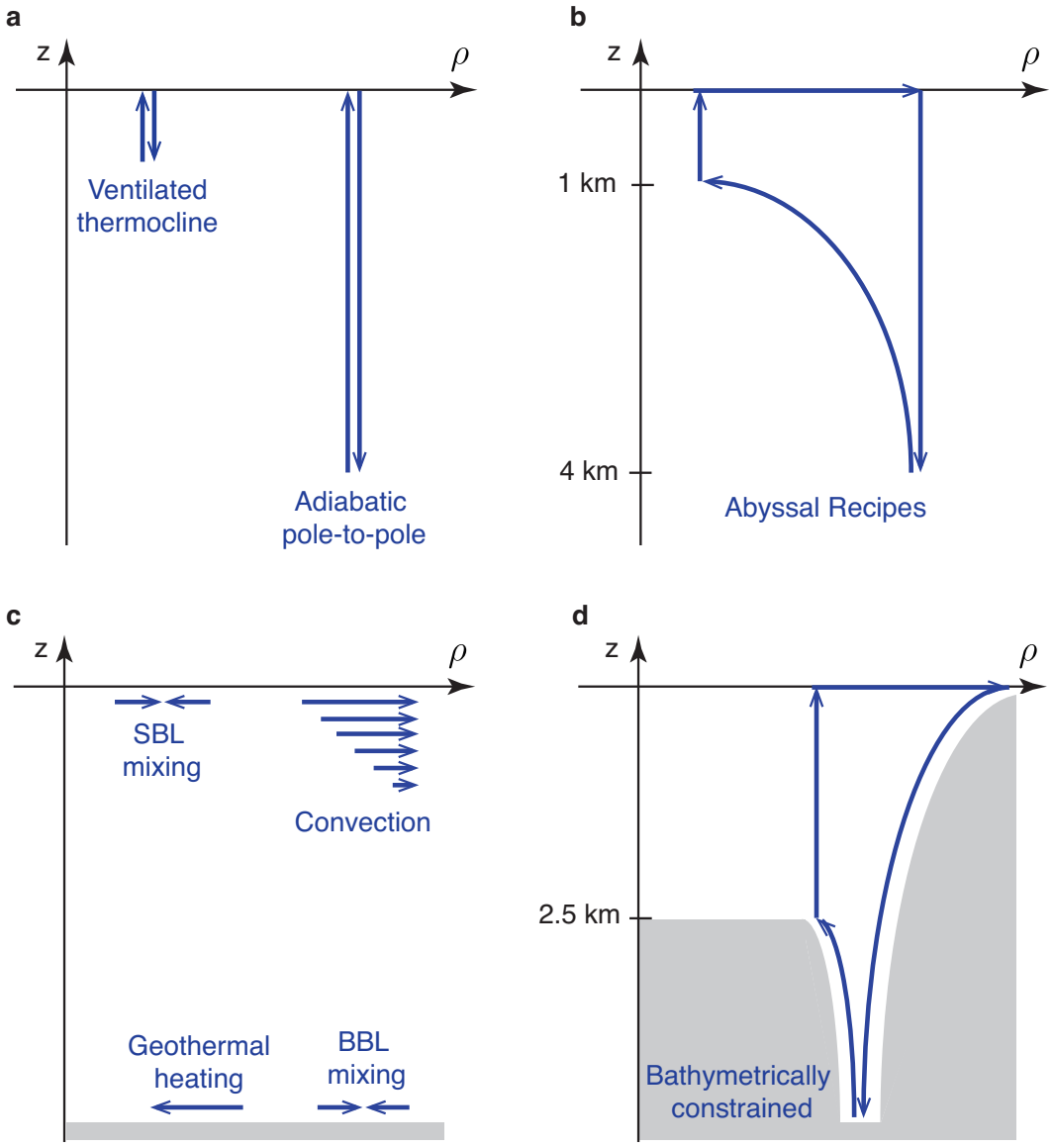

Figure 6: Idealized circulations viewed in density-depth coordinates. **a**, The ventilated thermocline (Luyten et al. 1983) and adiabatic pole-to-pole (Toggweiler and Samuels 1998, Wolfe and Cessi 2011) circulation frameworks involve flow along isopycnals only (with density transformations, i.e. movement along the x-axis, allowed only at the surface). **b**, The overturning circulation as modelled in the Abyssal Recipes of Munk and Wunsch (1998): dense waters sink at high latitudes down to 4 km depth and return to 1 km depth via mixing-driven upwelling across the low-latitude stratification. **c**, Schematic view of water parcel movements associated with mixing in the surface boundary layer (SBL), convective mixing forced by surface buoyancy loss, mixing in the bottom boundary layer (BBL), and geothermal heating. **d**, Proposed view of the overturning circulation: dense waters sink along the ocean floor, losing a large fraction of their density excess as they descend to abyssal depths and mix with overlying waters; mixing near the bottom and geothermal heating allows them to return to lighter layers up to 2.5 km depth; adiabatic Southern Ocean upwelling brings them from 2.5 km depth to the surface. The gray shading emphasizes the role of bathymetric constraints but does not imply that flow is disallowed within this phase space.

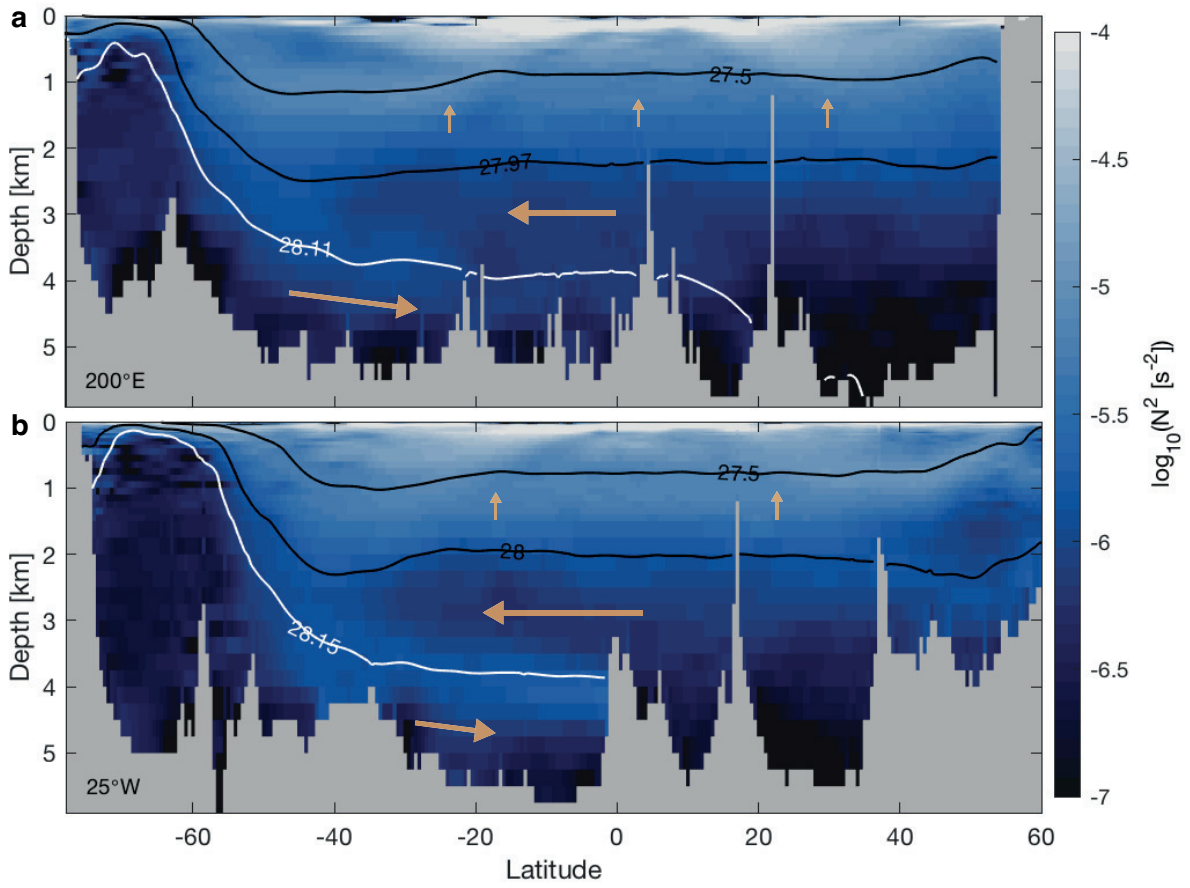

Figure 7: Squared buoyancy frequency ($N^2 = -\frac{g}{\rho}\frac{\partial \rho}{\partial z}$) along 200°E/160°W (**a**) and 25°W (**b**) transects cutting through the Pacific and Atlantic basins, respectively. Data from Gouretski and Koltermann (2004). Orange arrows illustrate the circulation implied by diapycnal transports diagnosed in Figure 8. In the Atlantic, the southward mid-depth flow is stronger than the bottom northward flow due to North Atlantic Deep Water inflow (Talley 2013, Lozier et al. 2019). White contours are the neutral density surfaces of meridional flow reversal, coinciding with a local stratification maximum. Black contours are density surfaces enclosing the Munk regime characterized by weak mixing-driven upwelling (see section 6a and Fig. 8). This regime's density range overlies that of abundant seafloor (de Lavergne et al. 2017; Fig. 12) and underlies that of intermediate waters (Naveira Garabato et al. 2014).

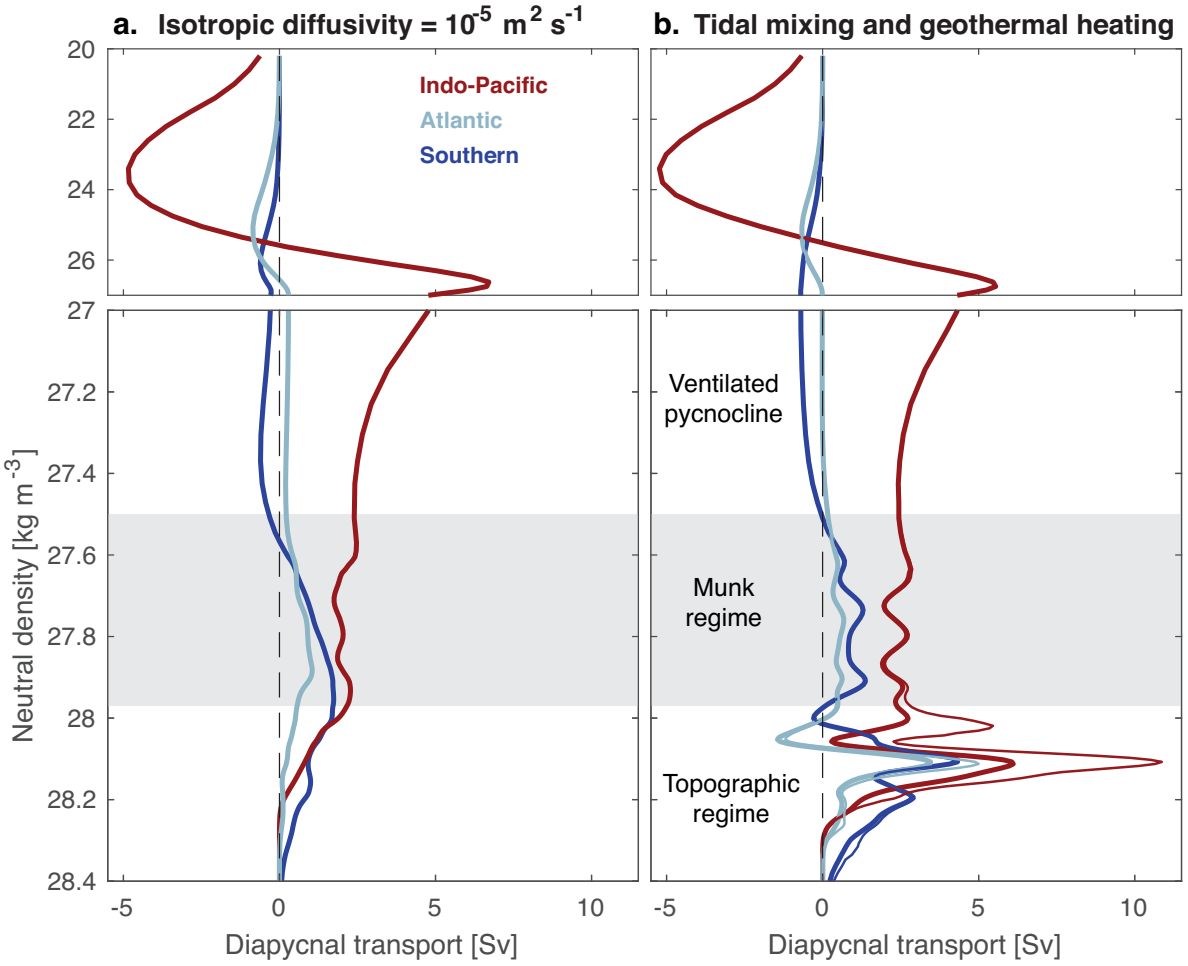

Figure 8: Estimated diapycnal upwelling due to isotropic mixing, split into Indo-Pacific (red), Atlantic (light blue) and Southern (dark blue) oceans. The Southern Ocean is defined as south of 32°S. **a**, Constant isotropic diffusivity of 10^{-5} m^2 s^{-1}. **b**, Realistic tidal mixing (thick curves), with added contribution of geothermal heating (thin curves). Positive values correspond to transport toward smaller densities (diapycnal upwelling). Where the shown transports increase upward, mixing causes volume loss or consumption; where transports decrease upward, mixing causes volume gain or formation. Regimes are defined in section 6 (see also Figs. 7 and 12). The employed climatological hydrography is that of Gouretski and Koltermann (2004). Tidal mixing rates are from de Lavergne et al. (2020) and geothermal heat fluxes from Lucazeau (2019). The methodology follows that of de Lavergne et al. (2016).

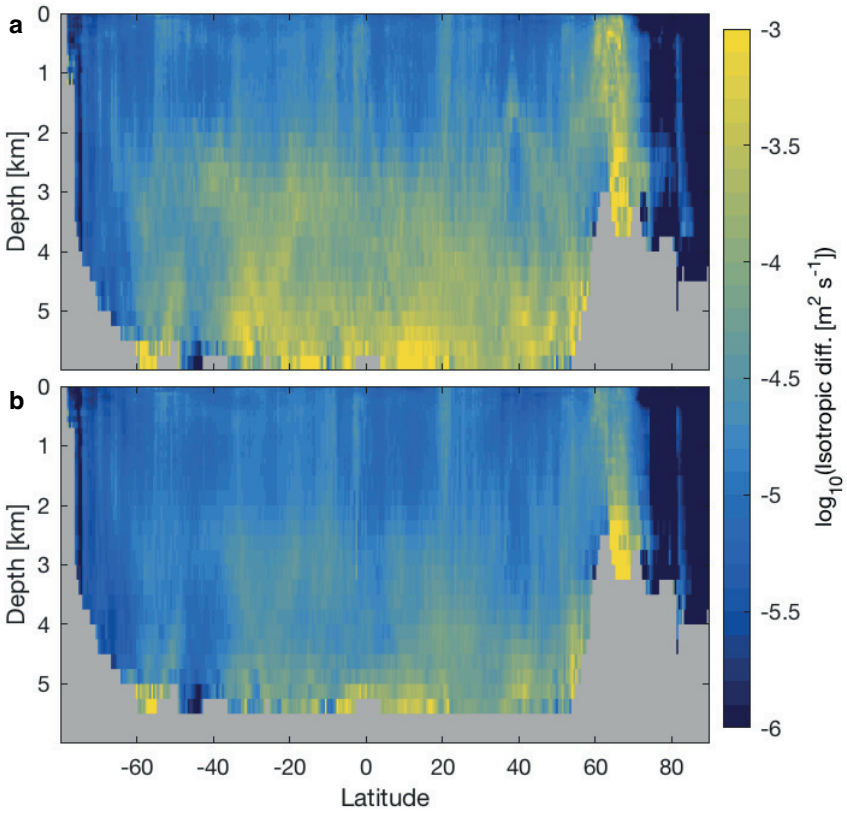

Figure 9: Zonal means of the isotropic diffusivity induced by internal tides, as mapped by de Lavergne et al. (2020). **a**, Global zonal mean diffusivity, where the average is weighted by $|\frac{\partial \rho}{\partial z}|$ so that mean values relate to density fluxes. **b**, Same as **a**, with the bottom 500 m of every water column excluded from the averaging.

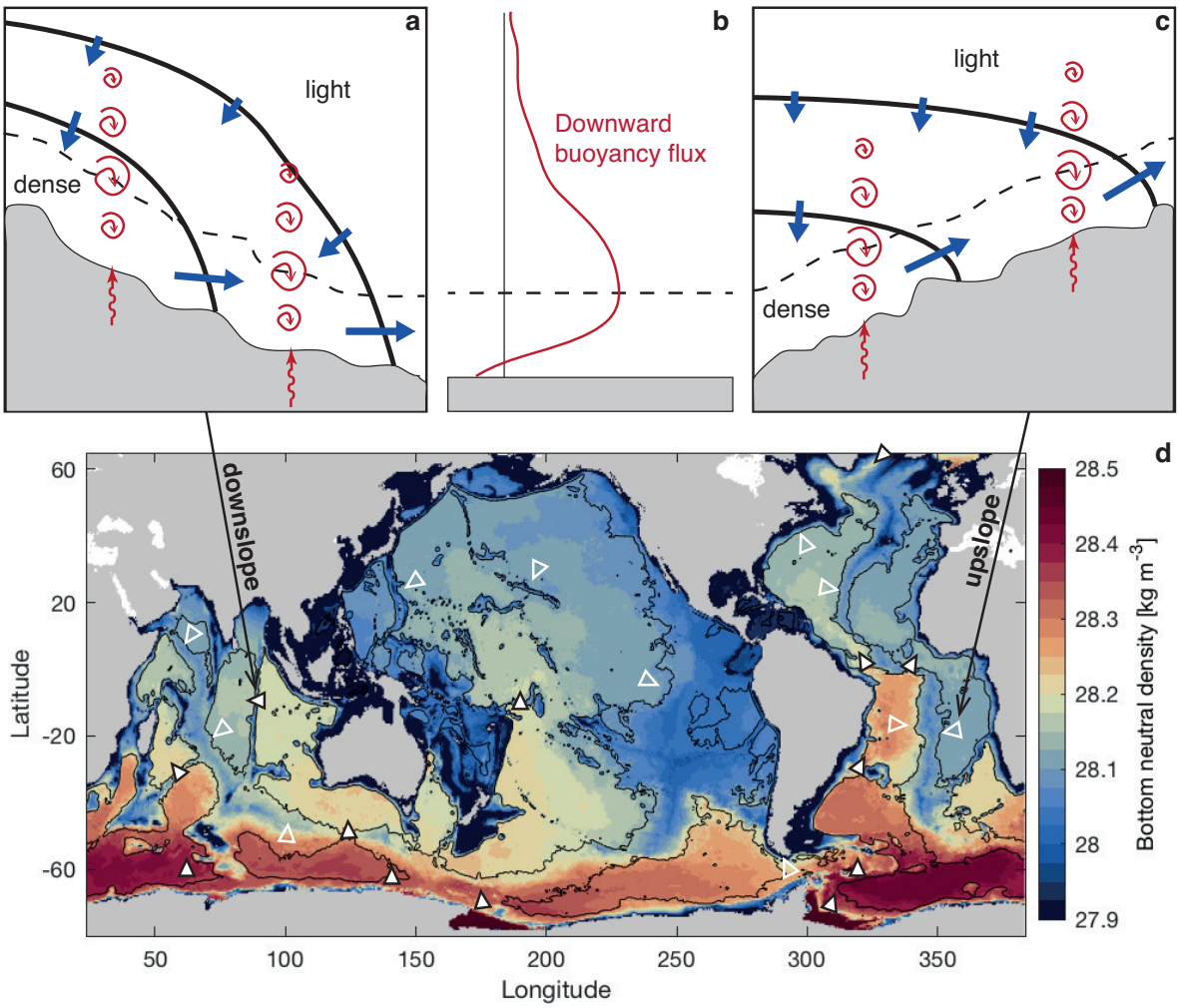

Figure 10: a-c, Downslope (**a**) and upslope (**c**) currents tied to near-bottom diffusive buoyancy fluxes (**b**). Boundary-catalyzed turbulence (red spirals) and geothermal heat fluxes (red wiggly arrows) drive a convergent buoyancy flux within a thin bottom layer (dashed line) and a divergent buoyancy flux above it. The bottom buoyancy gain is balanced by along-slope flow, whereas the buoyancy loss above is balanced by sinking of interior waters (blue arrows). Thick black lines represent density surfaces. **d**, For illustration, some representative locations of intense cross-density flows (triangles; filled for downslope, empty for upslope) are shown on top of shaded bottom neutral density (Gouretski and Koltermann 2004). The 4 km bathymetric contour is shown in black. Strong downslope flows filling the abyss are found downstream of major dense water formation sites and sills, while upslope cross-density transport is thought to be concentrated along the rough flanks of ridges.

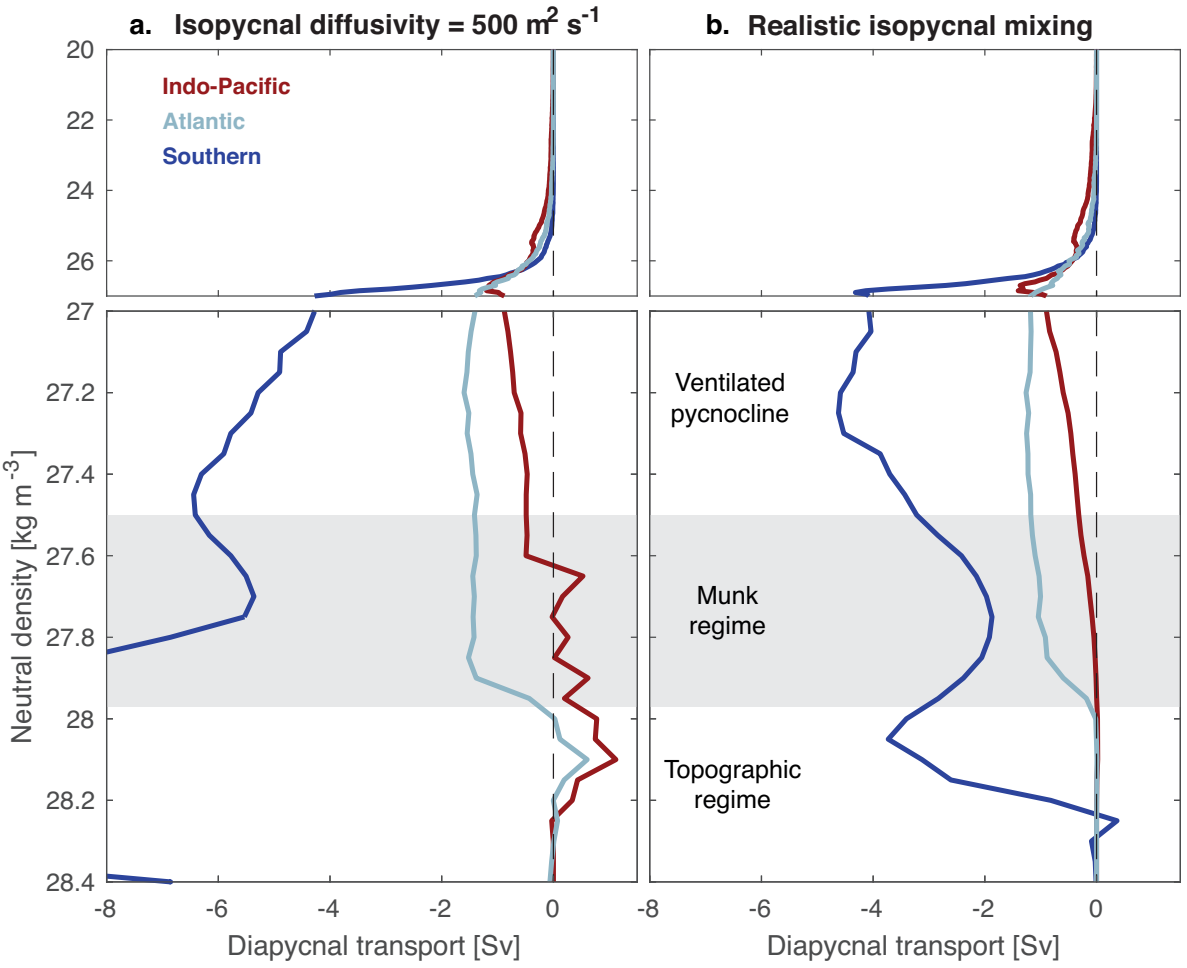

Figure 11: Estimated diapycnal upwelling due to isopycnal mixing, split into Indo-Pacific (red), Atlantic (light blue) and Southern (dark blue) oceans. The Southern Ocean is defined as south of 32°S. **a**, Constant isopycnal diffusivity of 500 m^2 s^{-1}. **b**, Varying isopycnal diffusivity mapped by Groeskamp et al. (2020). The calculation follows the methodology of Groeskamp et al. (2016) and is based on monthly climatological hydrographic fields from World Ocean Atlas 2018 (Locarnini et al. 2018, Zweng et al. 2018). Downwelling outside the axis range in panel **a**, at densities greater than 27.8 kg m^{-3}, occurs near the Antarctic continent and could be an artefact of poor observational coverage; more realistic diffusivities used in **b** eliminate these large transports.

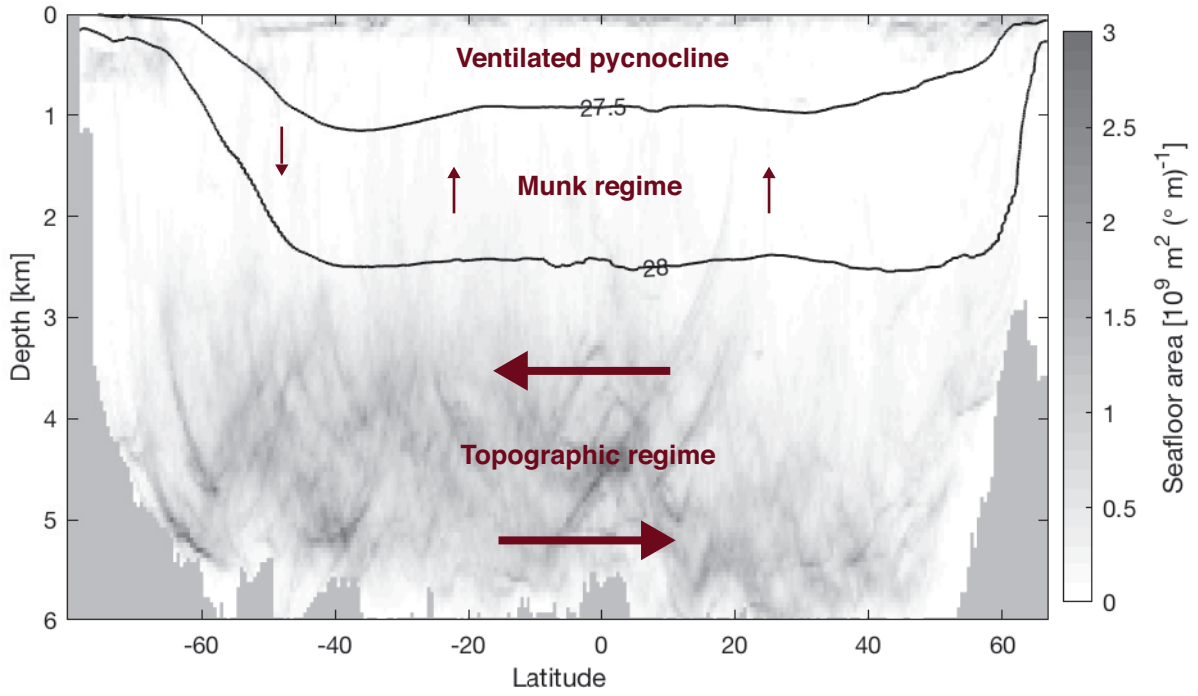

Figure 12: Proposed circulation regimes. The zonally summed seafloor area (in square meters per unit depth and per latitude degree) is shaded. Black curves represent the pseudo-depth of 27.5 and 28 kg m^{-3} neutral density surfaces, where the pseudo-depth of density surfaces is found by filling each latitude band from the bottom up with ocean grid cells ordered from dense to light. The Munk regime, between the two black contours, hosts moderate mixing-driven vertical circulation. The underlying topographic regime is characterized by northward abyssal flow and southward deep flow, both strongly influenced by topography and near-bottom mixing. The ventilated pycnocline hosts swift upper-ocean flows influenced by mixing near the surface.

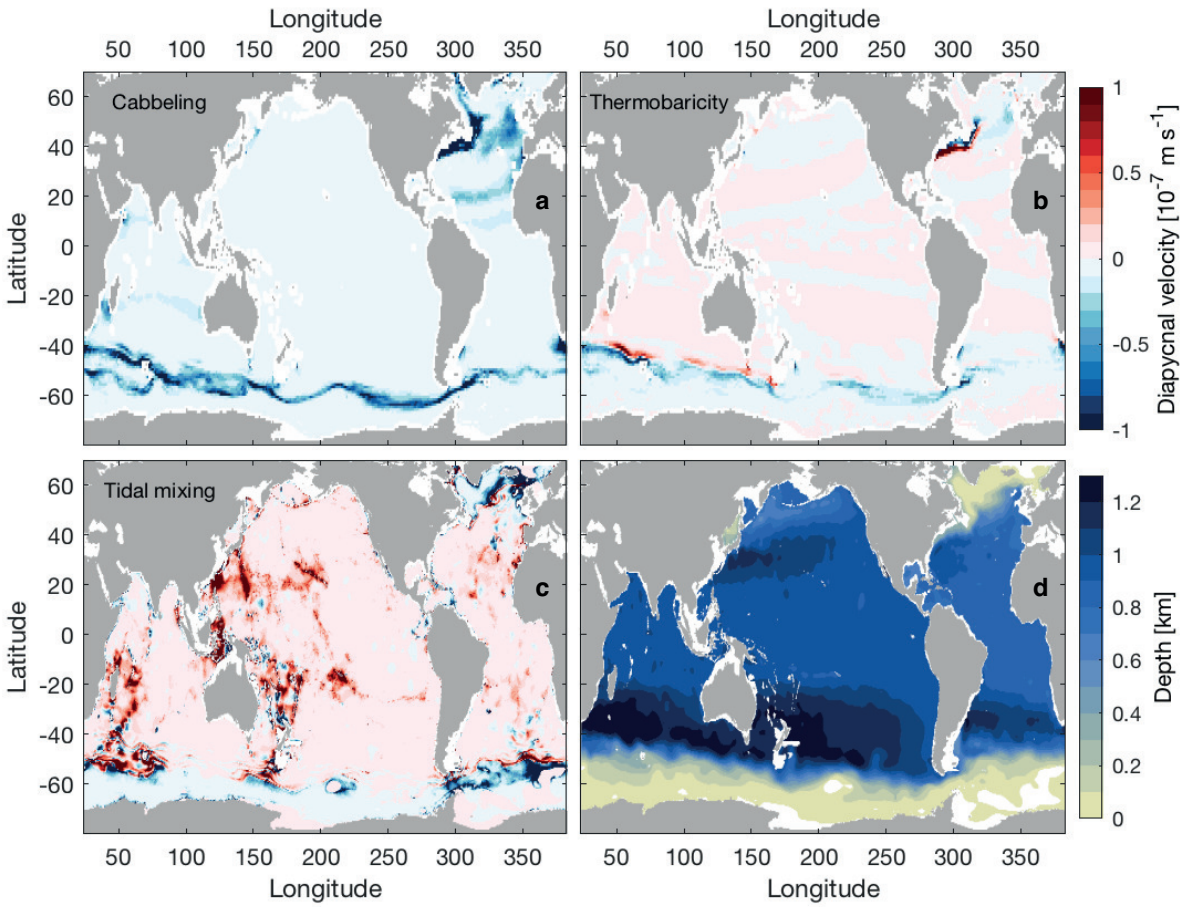

Figure 13: Estimated diapycnal velocities across the 27.5 kg m^{-3} surface. **a,b**, Velocity implied by isopycnal mixing via cabbeling (**a**) and thermobaricity effects (**b**), calculated according to Groeskamp et al. (2016), using World Ocean Atlas 2018 monthly hydrography (Locarnini et al. 2018, Zweng et al. 2018) and isopycnal diffusivities from Groeskamp et al. (2020). **c**, Velocity implied by tidal mixing calculated according to de Lavergne et al. (2016) using isotropic diffusivities from de Lavergne et al. (2020). **d**, Depth of the 27.5 kg m^{-3} neutral density surface in the climatology of Gouretski and Koltermann (2004). This density surface was chosen to separate the ventilated pycnocline from the Munk regime (Fig. 12).